nature cell biology

The *LINK-A* lncRNA activates normoxic HIF1α signalling in triple-negative breast cancer

Aifu Lin[1,13], Chunlai Li[1,13], Zhen Xing[1,13], Qingsong Hu[1], Ke Liang[1], Leng Han[2], Cheng Wang[3], David H. Hawke[4], Shouyu Wang[1], Yanyan Zhang[1], Yongkun Wei[1], Guolin Ma[5], Peter K. Park[1], Jianwei Zhou[6], Yan Zhou[7], Zhibin Hu[3], Yubin Zhou[5], Jeffery R. Marks[8], Han Liang[4,9], Mien-Chie Hung[1,10,11], Chunru Lin[1,10,14] and Liuqing Yang[1,10,12,14]

Although long non-coding RNAs (lncRNAs) predominately reside in the nucleus and exert their functions in many biological processes, their potential involvement in cytoplasmic signal transduction remains unexplored. Here, we identify a cytoplasmic lncRNA, *LINK-A* (long intergenic non-coding RNA for kinase activation), which mediates HB-EGF-triggered, EGFR:GPNMB heterodimer-dependent HIF1α phosphorylation at Tyr 565 and Ser 797 by BRK and LRRK2, respectively. These events cause HIF1α stabilization, HIF1α–p300 interaction, and activation of HIF1α transcriptional programs under normoxic conditions. Mechanistically, *LINK-A* facilitates the recruitment of BRK to the EGFR:GPNMB complex and BRK kinase activation. The BRK-dependent HIF1α Tyr 565 phosphorylation interferes with Pro 564 hydroxylation, leading to normoxic HIF1α stabilization. Both *LINK-A* expression and *LINK-A*-dependent signalling pathway activation correlate with triple-negative breast cancer (TNBC), promoting breast cancer glycolysis reprogramming and tumorigenesis. Our findings illustrate the magnitude and diversity of cytoplasmic lncRNAs in signal transduction and highlight the important roles of lncRNAs in cancer.

Triple-negative breast cancer (TNBC) continues to be a severe health problem[1–3], demanding the consideration of emerging long non-coding RNAs (lncRNAs) as biomarkers and therapeutic targets in combatting this disease[4–6]. Accumulating evidence demonstrates that lncRNAs have broad functional roles in the nucleus: regulation of transcriptional activation, X chromosome inactivation, heterochromatin formation, and maintenance of telomeres[7–14]. Alterations of these functions promote tumour formation, progression and metastasis of many cancer types[15–20]. However, many known lncRNAs reside either within the cytosol or shuttle between the nucleus and cytoplasm[21], playing important roles in modulating messenger RNA translation, decay and cytoplasmic protein trafficking[22–24]. Intriguingly, many protein kinases and metabolic enzymes bind RNA through their non-canonical RNA-binding domains[25–27], raising an important question of whether cytoplasmic lncRNAs are relevant in the regulation of fundamental cellular processes.

The hypoxia-inducible factor (HIF) transcriptional program is involved in TNBC progression, recurrence and metabolic reprogramming[28–30]. Although it is well known that the hydroxylation of HIF1α mediated by proline hydroxylase domain (PHD) proteins triggers VHL-dependent HIF1α ubiquitylation and degradation under normoxic conditions[31,32], under certain circumstances in tumour, HIF1α can accumulate under normoxic conditions, promoting angiogenesis and cancer progression[33,34]. However, the mechanism underlying normoxic HIF1α stabilization in TNBC remains elusive.

Here, we identified a highly prognostic lncRNA in TNBC, long intergenic non-coding RNA for kinase activation (*LINK-A*) (also known as *LOC339535* and NR_015407), which is critical for the growth factor-induced normoxic HIF1α signalling pathway.

[1]Department of Molecular and Cellular Oncology, The University of Texas M D Anderson Cancer Center, Houston, Texas 77030, USA. [2]Department of Biochemistry and Molecular Biology, The University of Texas Health Science Center at Houston McGroven Medical School, Houston, Texas 77030, USA. [3]Department of Epidemiology and Biostatistics and Ministry of Education (MOE), School of Public Health, Nanjing Medical University, 210029, China. [4]Department of System Biology, The University of Texas M D Anderson Cancer Center, Houston, Texas 77030, USA. [5]Center for Translational Cancer Research, Institute of Biosciences and Technology, Texas A&M University Health Science Center, Houston, Texas 77030, USA. [6]Department of Molecular Cell Biology and Toxicology, School of Public Health, Nanjing Medical University, 140 Hanzhong Road, Nanjing 210029, China. [7]Department of Oncology, Yixing People's Hospital, 75 Zhenguan Road, Yixing 214200, China. [8]Department of Surgery, Division of Surgical Science, Duke University, School of Medicine, Durham, North Carolina 27710, USA. [9]Department of Bioinformatics and Computational Biology, Division of Quantitative Sciences, The University of Texas M D Anderson Cancer Center, Houston, Texas 77030, USA. [10]The Graduate School of Biomedical Sciences, The University of Texas M D Anderson Cancer Center, Houston, Texas 77030, USA. [11]Center for Molecular Medicine and Graduate Institute of Cancer Biology, China Medical University, Taichung 404, Taiwan. [12]Center for RNA Interference and Non-Coding RNAs, The University of Texas M D Anderson Cancer Center, Houston, Texas 77030, USA. [13]These authors contributed equally to this work.
[14]Correspondence should be addressed to C.Lin or L.Y. (e-mail: clin2@mdanderson.org or lyang7@mdanderson.org)

Received 18 June 2015; accepted 30 November 2015; published online 11 January 2016; DOI: 10.1038/ncb3295

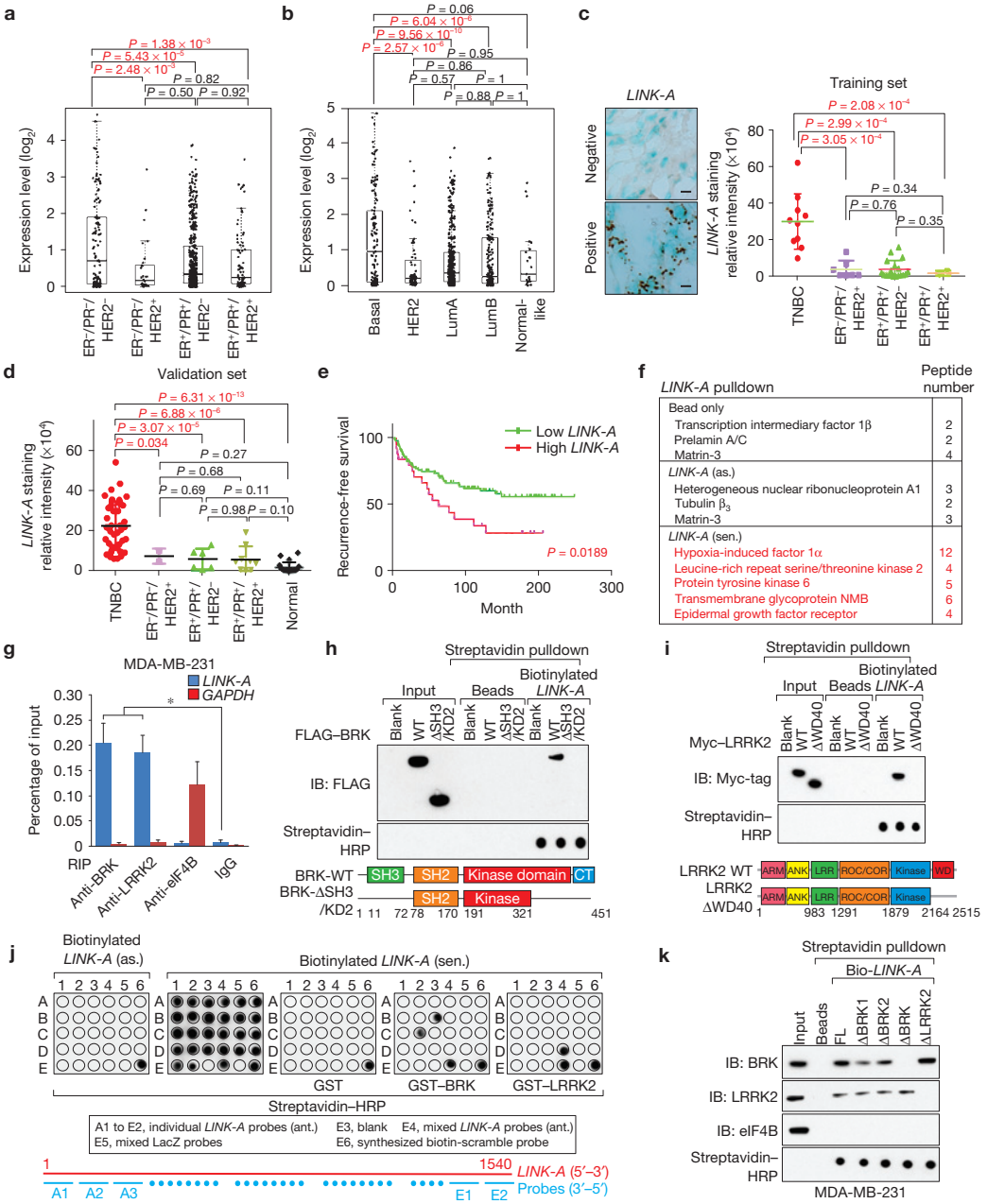

Figure 1 *LINK-A* is a TNBC-upregulated cytoplasmic lncRNA with prognostic value. (**a**,**b**) Scatter plots comparing *LINK-A* expression in breast tumour samples with different ER, PR and HER2 status including ER$^-$/PR$^-$/HER2$^-$ (n = 119), ER$^-$/PR$^-$/HER2$^+$ (n = 30), ER$^+$/PR$^+$/HER2$^-$ (n = 482), and ER$^+$/PR$^+$/HER2$^+$ (n = 80) (**a**), or in breast tumour tissue samples with different subtypes including basal (n = 139), HER2 (n = 67), LumA (n = 417), LumB (n = 191) and normal-like (n = 23) (**b**). Statistical significance was determined by two-way ANOVA. The boxes show the median and the interquartile range. The whiskers show the minimum and maximum. (**c**,**d**) RNAScope detection of *LINK-A* expression in human breast cancer and adjacent normal tissues (training (**c**) and validation (**d**) set, respectively). Left panel in **c**: representative images (scale bars, 100 μm); **d** and right panel in **c**: statistical analysis. Training set: TNBC (n = 10), ER$^-$/PR$^-$/HER2$^+$ (n = 7), ER$^+$/PR$^+$/HER2$^-$ (n = 18), and ER$^+$/PR$^+$/HER2$^+$ (n = 2); validation set: ER$^-$/PR$^-$/HER2$^-$ (n = 38), ER$^-$/PR$^-$/HER2$^+$ (n = 2), ER$^+$/PR$^+$/HER2$^-$ (n = 6), ER$^+$/PR$^+$/HER2$^+$ (n = 9) and normal tissue (n = 20) (median, two-way ANOVA). Horizontal black lines represent median. Coloured error bars represent 95% quantile. (**e**) Recurrence-free survival analysis of *LINK-A* status in breast cancer patients detected by qRT–PCR (n = 123 patients, Gehan–Breslow test). (**f**) A list of the top *LINK-A*-associated proteins identified by RNA pulldown and MS analysis in MDA-MB-231 cells. (**g**) RIP–qPCR detection of indicated RNAs retrieved by BRK-, LRRK2- or eIF4B-specific antibodies in MDA-MB-231 cells. Error bars, s.e.m., n = 3 independent experiments ($^*P < 0.05$, two-tailed paired Student's t-test). (**h**,**i**) *In vitro* RNA–protein binding assay showing the interaction of biotinylated *LINK-A* with wild-type (WT) FLAG-tagged BRK and a deletion mutant (**h**), or WT Myc-tagged LRRK2 and a deletion mutant (**i**). Dot-blot of RNA–protein binding samples indicates equal RNA transcript present in the assay. Bottom panel: graphic illustration of BRK or LRRK2 domain deletion mutants. IB, immunoblot. (**j**) Upper panel: *In vitro* RNA–protein binding followed by dot-blot assays using biotinylated *LINK-A* sense (sen.) or antisense (as.) transcripts and GST-tagged, bacterially expressed BRK or LRRK2 proteins. The hybridized RNA fragments were detected by streptavidin–HRP. Bottom panel: graphic illustration of *LINK-A* probes. (**k**) Immunoblot detection of proteins retrieved by *in-vitro*-transcribed biotinylated *LINK-A* full-length (FL) or deletion mutants expressed in MDA-MB-231 cells. Unprocessed original scans of blots are shown in Supplementary Fig. 7.

Mechanistically, *LINK-A* is required for HB-EGF-triggered, EGFR:GPNMB heterodimer-mediated recruitment of BRK to GPNMB, and subsequent enzymatic activation of BRK. The activated BRK, together with LRRK2 that is also recruited by *LINK-A*, phosphorylates HIF1α at Tyr 565 and Ser 797, respectively. Whereas the phosphorylation at Tyr 565 inhibits hydroxylation at the adjacent Pro 564, which prevents HIF1α degradation under normoxic conditions, Ser 797 phosphorylation facilitates HIF1α–p300 interaction, leading to activation of HIF1α target genes on HB-EGF stimulation. Furthermore, we demonstrated that LRRK2, a constitutively active kinase in Parkinson's disease, is a RNA-binding kinase that phosphorylates HIF1α in human cancers. Importantly, both *LINK-A* expression and activation of the *LINK-A*-mediated normoxic HIF1α signalling pathway correlated with TNBC. Therefore, targeting *LINK-A* may serve as a favourable strategy to block a normoxic HIF1α signalling pathway in TNBC with promising therapeutic potential.

RESULTS

LINK-A is a cytoplasmic lncRNA with prognostic value for TNBC

To identify TNBC-relevant lncRNAs, we examined the lncRNA expression profile in two stage III TNBC tissues and their paired adjacent non-cancerous tissues, finding 21 differentially expressed lncRNAs (ref. 16). We further searched the expression pattern of these 21 lncRNAs in the TCGA database. Interestingly, statistical analysis of a combined 711 RNA-seq transcriptome profiles indicated that the expression of *LINK-A* is frequently elevated in TNBC patient cohorts in comparison with cohorts of $ER^-/PR^-/HER2^+$, $ER^+/PR^+/HER2^-$ and $ER^+/PR^+/HER2^+$ patients. Differential *LINK-A* expression between $ER^-/PR^-/HER2^+$, $ER^+/PR^+/HER2^-$ and $ER^+/PR^+/HER2^+$ cohorts was not statistically significant (Fig. 1a). Consistently, basal-like breast cancer, which lacks or shows low levels of ER, PR and HER2 proteins[35,36], exhibited significantly increased *LINK-A* expression in comparison with $HER2^+$, LumA, LumB and normal-like subtypes (Fig. 1b).

LINK-A is a ~1.5-kb-long intergenic non-protein-coding RNA (ref. 37), which was confirmed by our northern blot and RACE analyses in MDA-MB-231 cells (Supplementary Fig. 1a,b). Given that *LINK-A* has a predicted open reading frame (ORF) of 139 amino acids, we performed *in vitro* translation assays, showing that neither the sense nor the antisense transcript of *LINK-A* encodes protein (Supplementary Fig. 1c). We next examined *LINK-A* expression in breast cancer tissue microarrays (clinicopathological parameters listed in Supplementary Table 1) using the RNAScope 2.0 HD assay. In both the training and validation sets of tissue samples, the expression of *LINK-A* was significantly increased in TNBC tissues compared with normal breast tissues, and $ER^-/PR^-/HER2^+$, $ER^+/PR^+/HER2^-$, and $ER^+/PR^+/HER2^+$ subtypes (Fig. 1c,d), demonstrating the strong correlation of *LINK-A* expression with TNBC. Additionally, we examined the *LINK-A* expression level in a Duke breast cancer cohort, finding that high levels of *LINK-A* correlated with unfavourable recurrence-free survival for breast cancer patients (Fig. 1e). Consistently, *LINK-A* was highly expressed in TNBC cell lines compared with oestrogen receptor (ER)- or HER2-positive breast cancer cell lines (Supplementary Fig. 1d).

Next, we examined the subcellular localization of *LINK-A*, finding that *LINK-A* predominately resides in the cytoplasm or close to the cellular membrane, which was distinct from typical nuclear lncRNAs including *BCAR4* (ref. 16) and *HOTAIR* (ref. 20) (Supplementary Fig. 1e–g). Cell fractionation analysis showed that >90% of *LINK-A* is localized within the cytosolic fraction compared with the nuclear enrichment of *BCAR4* (Supplementary Fig. 1h,i). We reasoned that *LINK-A* has important roles in the cytosol.

Identification and characterization of *LINK-A*–protein interaction

We performed an RNA pulldown assay followed by mass spectrometry[15,16] (MS) to identify *LINK-A*-associated proteins that might be involved in cytoplasmic processes. Interestingly, the sense *LINK-A*, but not the antisense or beads control, specifically associated with two transmembrane proteins, epidermal growth factor receptor (EGFR) and transmembrane glycoprotein NMB (GPNMB), tyrosine protein kinase 6 (also known as breast tumour kinase, BRK; refs 38,39), leucine-rich repeat kinase 2 (LRRK2; refs 40,41), and HIF1α in the breast cancer cell (Fig. 1f, Supplementary Fig. 1j and Supplementary Table 2). An RNA pulldown assay in cell lysate and an RNA–protein binding assay using recombinant EGFR, BRK, LRRK2, HIF1α and GPNMB confirmed that *LINK-A* associated with all of the proteins mentioned above *in vivo*, but only BRK and LRRK2 directly interacted with *LINK-A* (Supplementary Fig. 1k–n). The specific interaction between *LINK-A* and BRK or LRRK2 was also confirmed by an RNA immunoprecipitation (RIP) assay (Fig. 1g).

To map the BRK domains required for *LINK-A* binding, we generated BRK SH3 (amino acids 11–72), SH2 (amino acids 78–170), kinase domains (amino acids 191–445), and regulatory carboxy-terminal (amino acids 446–451) deletion mutants (Fig. 1h, bottom panel). Deletion of either the SH3 domain or the C-terminal region of the kinase domain of BRK alone impaired the interaction between *LINK-A* and BRK, suggesting that *LINK-A* interacts with two separate domains of BRK (Supplementary Fig. 1o). Double deletion of these two domains abolished the *LINK-A*–BRK interaction *in vitro* and *in vivo* (Fig. 1h and Supplementary Fig. 1p). A similar strategy was used to map the domain required for LRRK2–*LINK-A* interaction, showing that deletion of the WD40 domain, an atypical RNA-binding domain[16,25], abolished the direct interaction (Fig. 1i and Supplementary Fig. 1q).

To map RNA motifs essential for the *LINK-A*–protein interactions, we conducted an *in vitro* RNA–protein binding coupled with dot-blot assay[15,16], finding that BRK interacted with *LINK-A* at two regions, nucleotides 481–540 (dot B3) and nucleotides 781–840 (dot C2) (corresponding to the two domains of BRK at the SH3 domain and the C-terminal tail) (Fig. 1j). *LINK-A* nucleotides 1261–1320 (dot D4) interacted with LRRK2 (Fig. 1j). Consistently, double deletion of *LINK-A* (nucleotides 471–550 and nucleotides 771–850) abolished the BRK–*LINK-A* interaction without affecting the LRRK2–*LINK-A* interaction, whereas deletion of *LINK-A* (nucleotides 1251–1330) specifically abolished LRRK2–*LINK-A* association (Fig. 1k). The predicted secondary structure of *LINK-A* indicates that the RNA motifs required for BRK and LRRK2 interactions form individual branching stem loops,

a

Summary of phosphorylation sites identified from MS analysis

Protein	Site	Peptide sequence
GPNMB	Y525	K.EYNPIENSPGNVVR.S + phospho (Y)
BRK	Y351	K.EDVYLSHDHNIPYK.W + phospho (Y)
HIF1α	Y565	K.NPFSTQDTDLDLEMLAPYIPMDDDFQ LR.S + phospho (Y)
HIF1α	S797	R.LLGQSMDESGLPQLTSYDCEVNAPIQ GSR.N + phospho (ST)

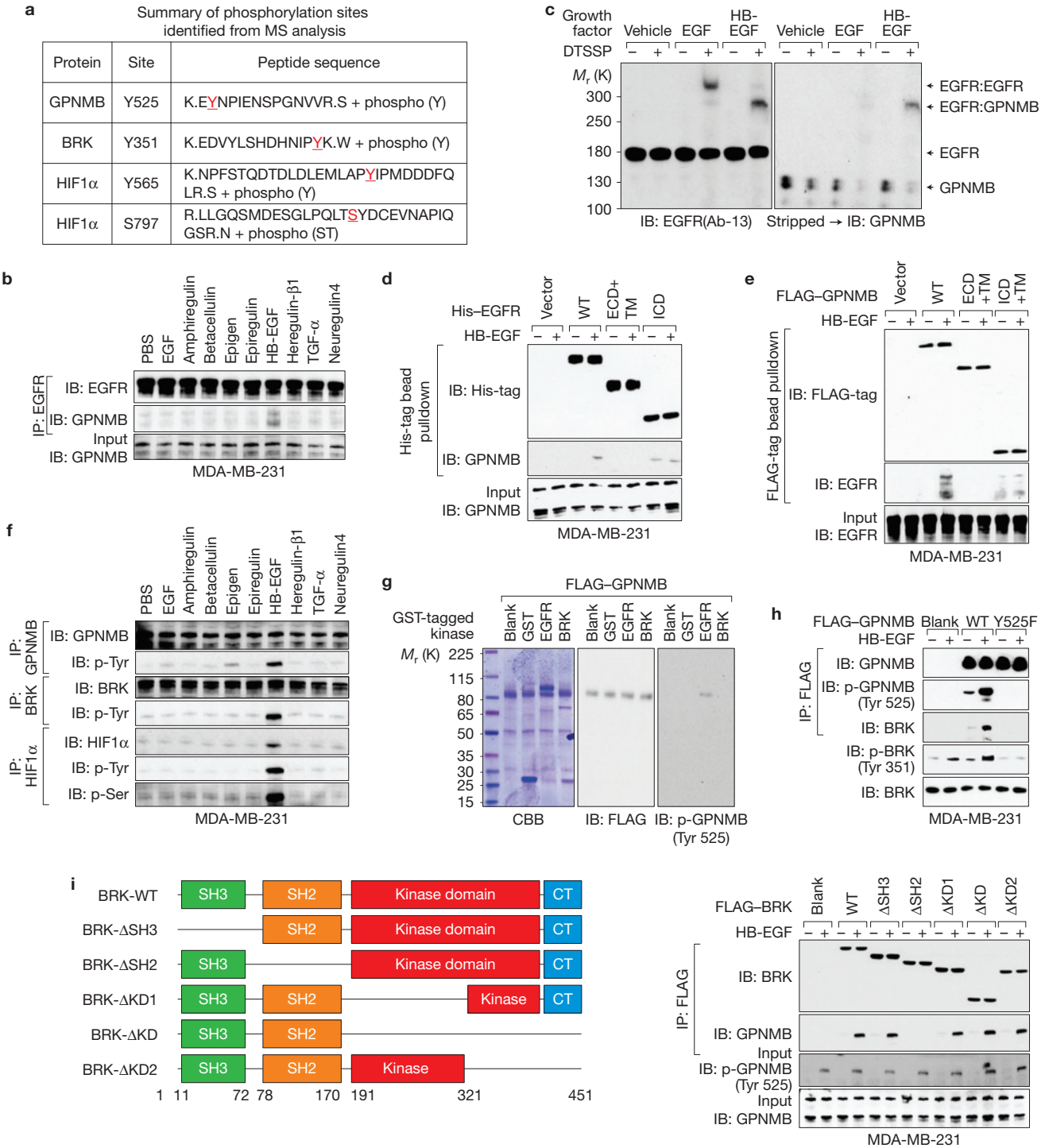

Figure 2 *LINK-A* is involved in an HB-EGF-triggered, EGFR:GPNMB-mediated signalling pathway. (**a**) Summary of the phosphorylation sites of the indicated proteins identified from RNA pulldown followed by MS analysis. (**b**) Immunoprecipitation (IP) followed by immunoblot (IB) detection of the indicated proteins in MDA-MB-231 cells treated with the indicated growth factors for 30 min. (**c**) Immunoblot detection using the indicated antibodies in MDA-MB-231 cells stimulated with vehicle, EGF or HB-EGF followed by DTSSP chemical crosslinking (1 mM, 30 min). (**d**,**e**) His tag (**d**) or FLAG tag (**e**) pulldown followed by immunoblot detection using the indicated antibodies in MDA-MB-231 cells transfected with the indicated expression vectors followed by HB-EGF stimulation. ECD, extracellular domain; TM, transmembrane domain; ICD, intracellular domain. (**f**) Immunoprecipitation followed by immunoblot detection of GPNMB, BRK and HIF1α phosphorylation in MDA-MB-231 cells treated with the indicated growth factors. (**g**) *In vitro* kinase assay using the indicated recombinant proteins, followed by Coomassie blue staining (CBB), and immunoblot detection using the indicated antibodies. (**h**,**i**) Immunoprecipitation followed by immunblot detection using the indicated antibodies in cells transfected with the indicated expression vectors followed by HB-EGF stimulation. Left panel (**i**): graphic illustration of BRK domain deletion mutants. Unprocessed original scans of blots are shown in Supplementary Fig. 7.

suggesting that they contribute to specific RNA–protein interactions (Supplementary Fig. 1r).

Characterization of a HB-EGF-triggered, EGFR:GPNMB-dependent and *LINK-A*-mediated signalling pathway in TNBC

Our MS data revealed a series of phosphorylation sites of GPNMB (Tyr 525), BRK (Tyr 351), and HIF1α (Tyr 565 and Ser 797) (Fig. 2a and Supplementary Fig. 2a–d and Supplementary Table 2), leading us to generate phosphorylation site-specific antibodies (Supplementary Fig. 2e–i) to investigate whether *LINK-A* modulates a previously unknown signalling pathway.

Given that *LINK-A* associated with the orphan receptor GPNMB and EGFR, which are involved in metastatic TNBC (refs 42–44), we reasoned that EGFR and GPNMB may interact with each other in TNBC cells on EGF family ligands. Although all EGFR ligands effectively activated EGFR (Supplementary Fig. 2j), HB-EGF robustly induced the specific interaction between EGFR and GPNMB (Fig. 2b), indicating that EGF ligands could differentially trigger the formation of the EGFR homodimer or the heterodimer between EGFR and other receptors[45]. To test this, we performed a crosslinking assay, finding that EGF predominately triggered EGFR homodimerization with a lesser degree of EGFR:GPNMB heterodimerization but HB-EGF stimulated EGFR:GPNMB heterodimerization with less EGFR homodimerization (Fig. 2c). Knockdown of *LINK-A* exhibited minimal effects on the HB-EGF-induced EGFR:GPNMB interaction as well as GPNMB phosphorylation on ligand stimulation (Supplementary Fig. 2k,l), suggesting that HB-EGF preferentially triggered EGFR:GPNMB heterodimer formation. We further mapped the domains mediating EGFR–GPNMB binding, and found that the kinase domain (KD) in EGFR intracellular domains (ICD) interacts with GPNMB ICD (Fig. 2d,e and Supplementary Fig. 2m). HB-EGF robustly induced site-specific phosphorylation of EGFR, GPNMB, BRK and HIF1α (Fig. 2f) and pretreatment of TNBC cell lines with cetuximab impaired EGFR–GPNMB interaction (Supplementary Fig. 2n,o). These observations led us to fully characterize this HB-EGF-triggered, EGFR:GPNMB-dependent signalling pathway in TNBC.

First, an *in vitro* kinase assay indicated that EGFR, but not BRK, phosphorylated GPNMB at Tyr 525 (Fig. 2g) and the exogenously expressed wild-type GPNMB but not the Y525F mutant was phosphorylated *in vivo* on HB-EGF stimulation (Fig. 2h). Next, we observed the interaction between GPNMB and BRK following ligand stimulation, which was abolished in the presence of the GPNMB Y525F mutant (Fig. 2h). Furthermore, the ligand-triggered BRK Tyr 351 phosphorylation was abolished in GPNMB Y525F-overexpressing cells (Fig. 2h). Biochemical experiments showed that BRK SH2 domain deletion (amino acids 78–170) eliminated the ligand-dependent interaction with Tyr-525-phosphorylated GPNMB (Fig. 2i). These data suggest that the EGFR-dependent GPNMB Tyr 525 phosphorylation is required for further recruitment of BRK through its SH2 domain and subsequent phosphorylation at Tyr 351.

LINK-A facilitates the recruitment and activation of BRK

We then conducted an immuno-RNA fluorescence *in situ* hybridization (FISH) assay to examine the proximity of *LINK-A* to the ligand-bound receptors on ligand treatment, finding the overlap between *LINK-A* and EGFR on HB-EGF stimulation (Supplementary Fig. 3a), which was further validated by *in vivo* RIP assay (Supplementary Fig. 3b). We examined the co-localization of BRK and the EGFR:GPNMB receptor complex in the presence or absence of *LINK-A*. Our data indicate that both BRK and phospho-BRK (Tyr 351) faithfully co-localized with EGFR on HB-EGF stimulation (Fig. 3a and Supplementary Fig. 3c). In contrast, depletion of *LINK-A* abolished the recruitment of BRK to EGFR and subsequent phosphorylation of BRK without affecting the internalization of EGFR (Fig. 3a and Supplementary Fig. 3c). We then performed rescue experiments in which *LINK-A* was knocked down by locked nucleic acids (LNAs) followed by reintroduction of LNA-resistant full-length *LINK-A* or one of the following deletion mutants: ΔBRK (Δ471–550 and Δ771–850) or ΔLRRK2 (Δ1251–1330) (Fig. 3b, lower panel, and Supplementary Fig. 3d,e), finding that knockdown of *LINK-A* abolished the HB-EGF-induced BRK–GPNMB interaction, as well as BRK Tyr 351 phosphorylation (Fig. 3c,d); reintroduction of full-length *LINK-A* or ΔLRRK2 but not the ΔBRK mutant rescued these phenotypes (Fig. 3c,d). These data suggest that *LINK-A*–BRK interaction facilitates the recruitment of BRK to the tyrosine-phosphorylated membrane receptor GPNMB, as well as subsequent autophosphorylation of BRK.

LINK-A elicits the conformational change of BRK for kinase activation

It has been reported that the activity of BRK is auto-inhibited by interaction between the SH2 domain and the Tyr-447-phosphorylated C-terminal domain[46–48]. Our data indicate that *LINK-A* interacts with BRK at two regions, the SH3 domain and the C-terminal domain (see Fig. 1h and Supplementary Fig. 1p), raising a possible role for *LINK-A* in eliciting a BRK conformational change that mitigates the conformation required for self-inhibition. Indeed, we found that full-length *LINK-A* and ΔLRRK2 *LINK-A* markedly enhanced the autophosphorylation and kinase activity of BRK, whereas both the control lncRNA and ΔBRK *LINK-A* showed minimal effects (Fig. 3e,f).

We next conducted a protease digestion assay by incubating BRK with caspase-1 in the presence of full-length *LINK-A* or ΔBRK *LINK-A*, finding that caspase-1 barely cleaved BRK at amino acid 397 in the presence of an unrelated lncRNA *RP11-383G10.5*, but robustly cleaved BRK only in the presence of full-length *LINK-A* (Fig. 3g), suggesting that a potential conformational change occurred in BRK to expose the digestion site on *LINK-A* binding. Notably, deletion of either of the two regions of *LINK-A* involved in BRK interaction failed to promote the caspase-1-dependent BRK cleavage (Fig. 3g), suggesting that simultaneous binding of *LINK-A* to the two BRK domains is required to elicit the conformational change in BRK. Our data suggest that the binding of *LINK-A* to BRK promotes a conformational change, leading to increased accessibility of the SH2 domain and the autophosphorylation sites in the kinase domain. On ligand stimulation, these events lead to the recruitment of BRK to Tyr-525-phosphorylated GPNMB and activation of BRK on Tyr 351 phosphorylation.

LINK-A-interacting BRK and LRRK2 phosphorylate HIF1α

We next performed *in vitro* phosphorylation assays, finding that activated BRK phosphorylated HIF1α at Tyr 565 (Fig. 4a) and

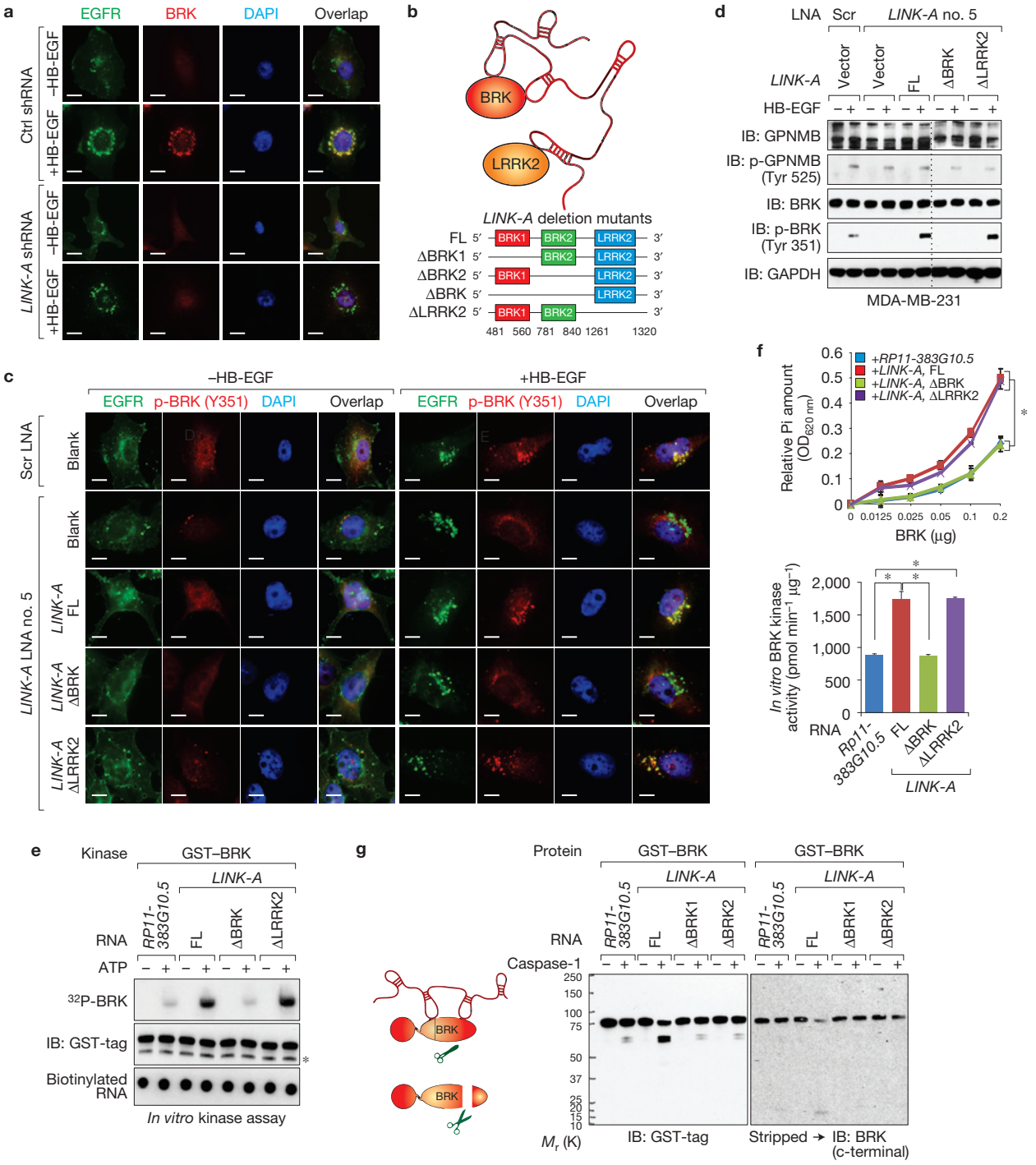

Figure 3 *LINK-A* mediates recruitment of BRK to GPNMB for kinase activation. (**a**) Immunofluorescence detection using the indicated antibodies in MDA-MB-231 cells harbouring control (upper panel) or *LINK-A* shRNA, followed by HB-EGF stimulation (upper panel). Scale bars, 20 μm. (**b**) Graphic illustration of the BRK– and LRRK2–*LINK-A* interactions (upper panel) and the corresponding deletion abolishing these interactions (lower panel). (**c**,**d**) Immunofluorescence imaging (**c**, scale bars, 20 μm) or immunoblot (IB) detection (**d**) was performed using the indicated antibodies in MDA-MB-231 cells transfected with LNA against *LINK-A* followed by overexpression of the indicated rescue plasmids with HB-EGF stimulation. The dotted line on the blots of **d** indicates the position where the images of single blots were vertically cropped to juxtapose non-adjacent lanes. (**e**) *In vitro* kinase assay using recombinant BRK and *in vitro*-transcribed RNA transcripts as indicated in the presence or absence of [32P]ATP. The dot-blot indicates equal RNA transcript present in the assay. (**f**) Quantification of BRK kinase activity in the presence of the indicated *in vitro*-transcribed RNA transcripts using HIF1α peptide (amino acids 557–566) as the substrate. Upper panel: release of free phosphate ion (P_i) amount measured at OD_{620nm}; lower panel: calculation of BRK kinase activity (pmol min^{-1} μg^{-1}). Error bars, s.e.m., $n = 3$ independent experiments ($^*P < 0.05$, two-tailed paired Student's *t*-test). (**g**) Immunblot detection of BRK using the indicated antibodies in the presence of the indicated lncRNA transcripts with or without caspase-1 digestion. Left panel: graphic illustration of caspase-1-mediated BRK cleavage in the absence or presence of lncRNA. Unprocessed original scans of blots are shown in Supplementary Fig. 7.

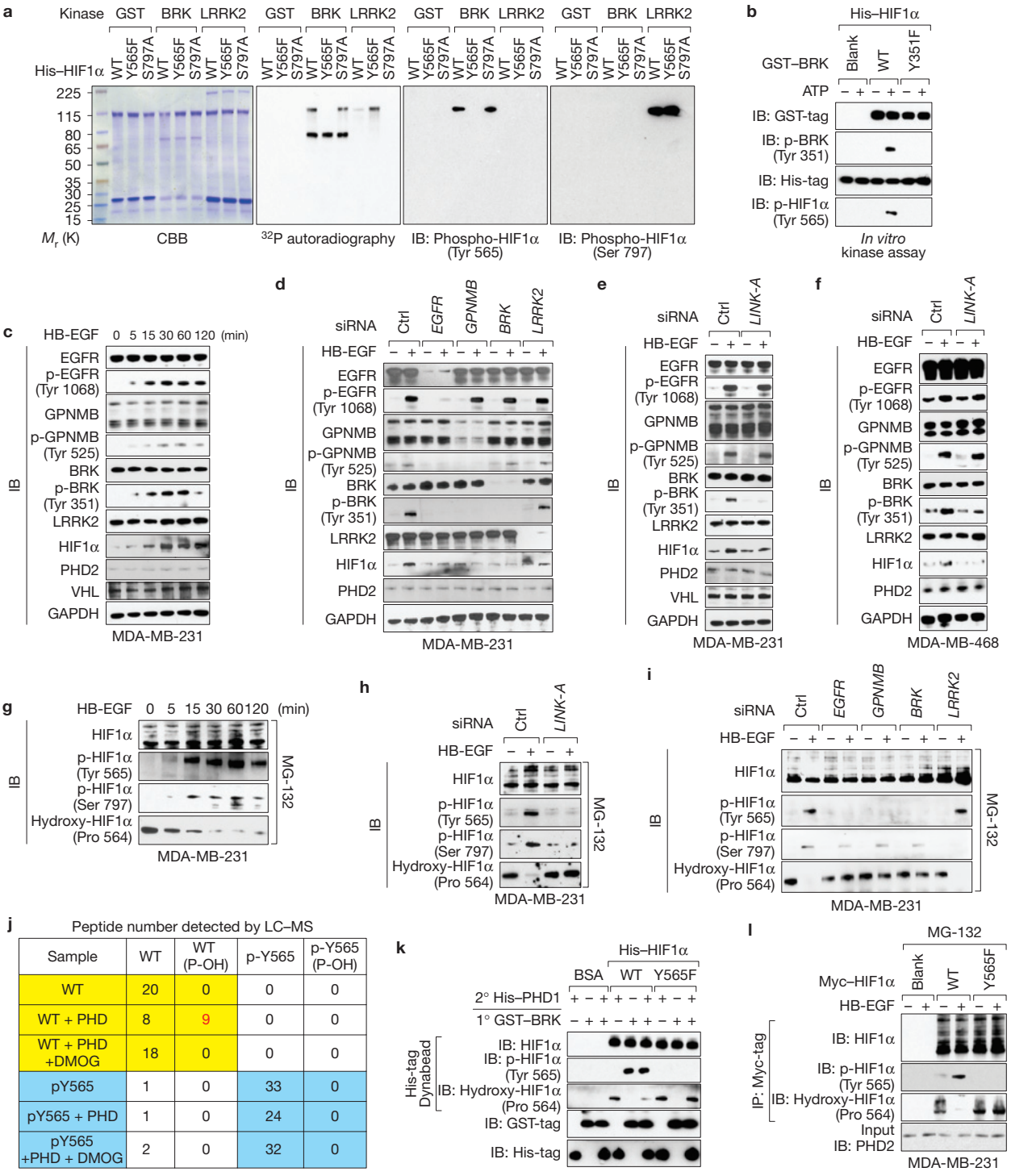

Sample	WT	WT (P-OH)	p-Y565	p-Y565 (P-OH)
WT	20	0	0	0
WT + PHD	8	9	0	0
WT + PHD +DMOG	18	0	0	0
pY565	1	0	33	0
pY565 + PHD	1	0	24	0
pY565 +PHD + DMOG	2	0	32	0

Figure 4 *LINK-A*-dependent BRK phosphorylation of HIF1α at Tyr 565 antagonizes HIF1α Pro 564 hydroxylation. (**a**) *In vitro* phosphorylation assay using recombinant proteins (WT or mutants as indicated). IB, immunblot. (**b**) *In vitro* kinase assay using bacterially expressed GST-tagged BRK WT or mutant and His-tagged HIF1α. (**c**–**f**) Immunoblot detection using the indicated antibodies in MDA-MB-231 (**c**–**e**) or MDA-MB-468 (**f**) cells treated with HB-EGF at the indicated time point (**c**) or transfected with the indicated siRNAs followed by HB-EGF treatment (**d**–**f**). (**g**–**i**) Immunoblot detection using the indicated antibodies in MDA-MB-231 cells treated with MG-132 followed by HB-EGF treatment at the indicated time (**g**) or in cells transfected with the indicated siRNAs followed by MG-132 and HB-EGF treatment (**h**,**i**). (**j**) LC–MS sequencing of the HIF1α peptide (557–566) in an *in vitro* hydroxylation assay. The total peptide numbers of HIF1α proline non-hydroxylated versus proline hydroxylated (P-OH) under the indicated conditions are shown. The peptide number of hydroxylated WT peptide is indicated in red. (**k**) His-tag pulldown followed by immunoblot detection of HIF1α phosphorylation and hydroxylation (WT versus Y565F) in an *in vitro* kinase assay (1°) followed by *in vitro* hydroxylation assay (2°). (**l**) Immunoprecipitation (IP) followed by immunoblot detection of HIF1α phosphorylation and hydroxylation (WT versus Y565F) in MDA-MB-231 cells transfected with the indicated plasmids and treated with MG-132 followed by HB-EGF treatment. Unprocessed original scans of blots are shown in Supplementary Fig. 7.

LRRK2, another *LINK-A*-interacting protein kinase, phosphorylated HIF1α at Ser 797, which was further demonstrated by the marked inhibition of HIF1α phosphorylation in the presence of a S797A point mutant (Fig. 4a). The BRK kinase activity-deficient mutant, Y351F, diminished the phosphorylation of HIF1α *in vivo* (Fig. 4b). Both Tyr 565 and Ser 797 of HIF1α are conserved (Supplementary Fig. 4a).

HB-EGF induced phosphorylation of GPNMB (Tyr 525) and BRK (Tyr 351), as well as HIF1α protein stabilization under normoxic conditions (Fig. 4c and Supplementary Fig. 4b). Interestingly, knockdown of EGFR abolished the ligand-dependent phosphorylation of GPNMB (Tyr 525) and BRK (Tyr 351), as well as the stabilization of HIF1α; knockdown of GPNMB abolished HB-EGF-induced BRK phosphorylation and HIF1α protein stabilization, but did not affect EGFR phosphorylation (Tyr 1068) (Fig. 4d). Knockdown of *LINK-A* in both MDA-MB-231 and MDA-MB-468 cells eliminated HB-EGF-induced BRK phosphorylation and HIF1α stabilization, but not phosphorylation of EGFR or GPNMB (Fig. 4e,f). In contrast, *LINK-A* knockdown exhibited minimal effects on hypoxia-dependent HIF1α stabilization, and hypoxia failed to trigger phosphorylation of GPNMB and BRK (Fig. 4c–f and Supplementary Fig. 4c). Finally, depletion of BRK decreased ligand-triggered HIF1α protein accumulation but did not affect the phosphorylation status of EGFR or GPNMB (Fig. 4d). Taken together, these data suggest a linear EGFR:GPNMB→*LINK-A*→BRK/LRRK2→HIF1α signalling cascade on HB-EGF stimulation under normoxic conditions.

On HB-EGF stimulation, HIF1α underwent Tyr 565 and Ser 797 phosphorylation but the hydroxylation at Pro 564 was inhibited, which led to HIF1α stabilization (Fig. 4g). Knockdown of *LINK-A* abolished HB-EGF-induced HIF1α Tyr 565 phosphorylation and enhanced the Pro 564 hydroxylation (Fig. 4h and Supplementary Fig. 4d). A similar pattern was observed with EGFR, GPNMB and BRK knockdown (Fig. 4i). These data suggest that HB-EGF triggers an lncRNA-dependent signalling pathway to stabilize HIF1α at the protein level.

Tyr 565 phosphorylation antagonizes Pro 564 hydroxylation to stabilize HIF1α under normoxia

An *in vitro* hydroxylation assay demonstrated that the HIF1α peptides (amino acids 557–566) but not Tyr-565-phosphorylated peptides can be hydroxylated by PHD1 (Fig. 4j and Supplementary Fig. 4e–j and Supplementary Table 3). An *in vitro* kinase assay followed by an *in vitro* hydroxylation assay further showed that phosphorylation of wild-type HIF1α but not the Y565F mutant by BRK prevented subsequent hydroxylation at Pro 564 (Fig. 4k). Consistently, HB-EGF-triggered Tyr 565 phosphorylation of HIF1α and inhibition of hydroxylation at Pro 564, which was abolished by overexpression of the Y565F mutant of HIF1α (Fig. 4l).

A cycloheximide treatment experiment revealed that on HB-EGF stimulation, the HIF1α protein exhibited ≥4 h half-life but knocking down *LINK-A* reduced it to 1.5 h (Supplementary Fig. 4k,l). In TNBC cells exogenously expressing wild-type HIF1α or the Y565D mutant, the Y565D mutant exhibited a constitutively prolonged half-life (Supplementary Fig. 4m–o). These data indicate that *LINK-A*-associated BRK phosphorylated HIF1α at Tyr 565, which prevents HIF1α hydroxylation at adjacent Pro 564 and stabilizes HIF1α under normoxia.

LINK-A-recruited LRRK2 phosphorylates Ser 797 of HIF1α to potentiate its transcriptional activity

Knockdown of *LINK-A* or LRRK2, or overexpression of the HIF1α S797A mutant abolished Ser 797 phosphorylation of HIF1α as well as its association with p300, which was concurrent with the release of FIH (ref. 49), a protein that binds to HIF1α and inhibits its trans-activation function (Fig. 5a,b). We also examined the kinase activity of LRRK2 in the presence of *LINK-A*, finding that full-length *LINK-A*, ΔBRK *LINK-A* or ΔLRRK2 *LINK-A* exhibited minimal effect on the kinase activity of LRRK2 (Supplementary Fig. 5a). The rescue experiments indicated that full-length *LINK-A* fully rescued HIF1α phosphorylation and protein stabilization; ΔBRK *LINK-A* rescued only HIF1α Ser 797 phosphorylation and ΔLRRK2 *LINK-A* restored HIF1α Tyr 565 phosphorylation and protein stabilization, but failed to rescue the phosphorylation of HIF1α at Ser 797 (Fig. 5c). Recent studies have shown that certain lncRNAs encode small protein peptides[50–52]. Whereas our data have demonstrated that a predicted ORF of *LINK-A* has no protein-coding products *in vitro* (see Supplementary Fig. 1a–c), we further mutated the predicted translational start codon ATG (nucleotides 318–321), or the potential stop codon TGA (nucleotides 732–735), of this ORF in a functional rescue experiment, finding that the phosphorylation of BRK (Tyr 351) and HIF1α (Tyr 565), two major cellular effects mediated by *LINK-A*, was fully rescued by wild-type *LINK-A* as well as ATG→TAG or TGA→TGT mutants of *LINK-A* (Supplementary Fig. 5b–d). These observations suggested that the cellular effect of *LINK-A* is mainly dependent on its RNA function instead of the potential translational products. Taken together, we demonstrated that *LINK-A*, in coordination with two protein kinases BRK and LRRK2, mediated a growth factor-triggered signalling cascade to synergistically regulate the phosphorylation and protein stabilization of HIF1α under normoxia.

LINK-A-dependent normoxic HIF1α signalling promotes tumour growth and correlates with TNBC

Next, we examined the transcriptional activity of HIF1α on HB-EGF stimulation by ChIP-seq, finding that under normoxia, HB-EGF triggered the recruitment of HIF1α to the promoters of HIF1α target genes and regulated the HIF1α-dependent transcriptional program (Fig. 5d,e and Supplementary Table 4). Knockdown of *LINK-A* in TNBC cells impaired HIF1α-target gene expression on HB-EGF stimulation (Fig. 5f,g and Supplementary Fig. 5e). Consistently, *in vitro* glucose uptake and lactate production assays confirmed that *LINK-A* deficiency impaired glycolysis (Supplementary Fig. 5f–l). Consistent with the *in vitro* colony formation assays (Fig. 5h), mice with xenografts of *LINK-A*-depleted tumour cells rarely developed tumour mass *in vivo* (Fig. 5i,j and Supplementary Fig. 5m).

The *LINK-A*-mediated signalling pathway was also activated in TNBC tissues, as evidenced by a significantly higher staining density of phospho-GPNMB (Tyr 525), phospho-BRK (Tyr 351), phospho-HIF1α (Tyr 565) and phospho-HIF1α (Ser 797) in TNBC samples compared with non-TNBC samples (Fig. 6a–c and Supplementary Fig. 6a). Furthermore, within the TNBC category, breast cancer with advanced lymph-node metastasis showed increased phospho-BRK (Tyr 351), phospho-HIF1α (Tyr 565) and phospho-GPNMB (Tyr 525) levels compared with tissue samples with no lymph-node metastasis (Fig. 6a–c,d–f, upper panel). Importantly, there is a strong correlation

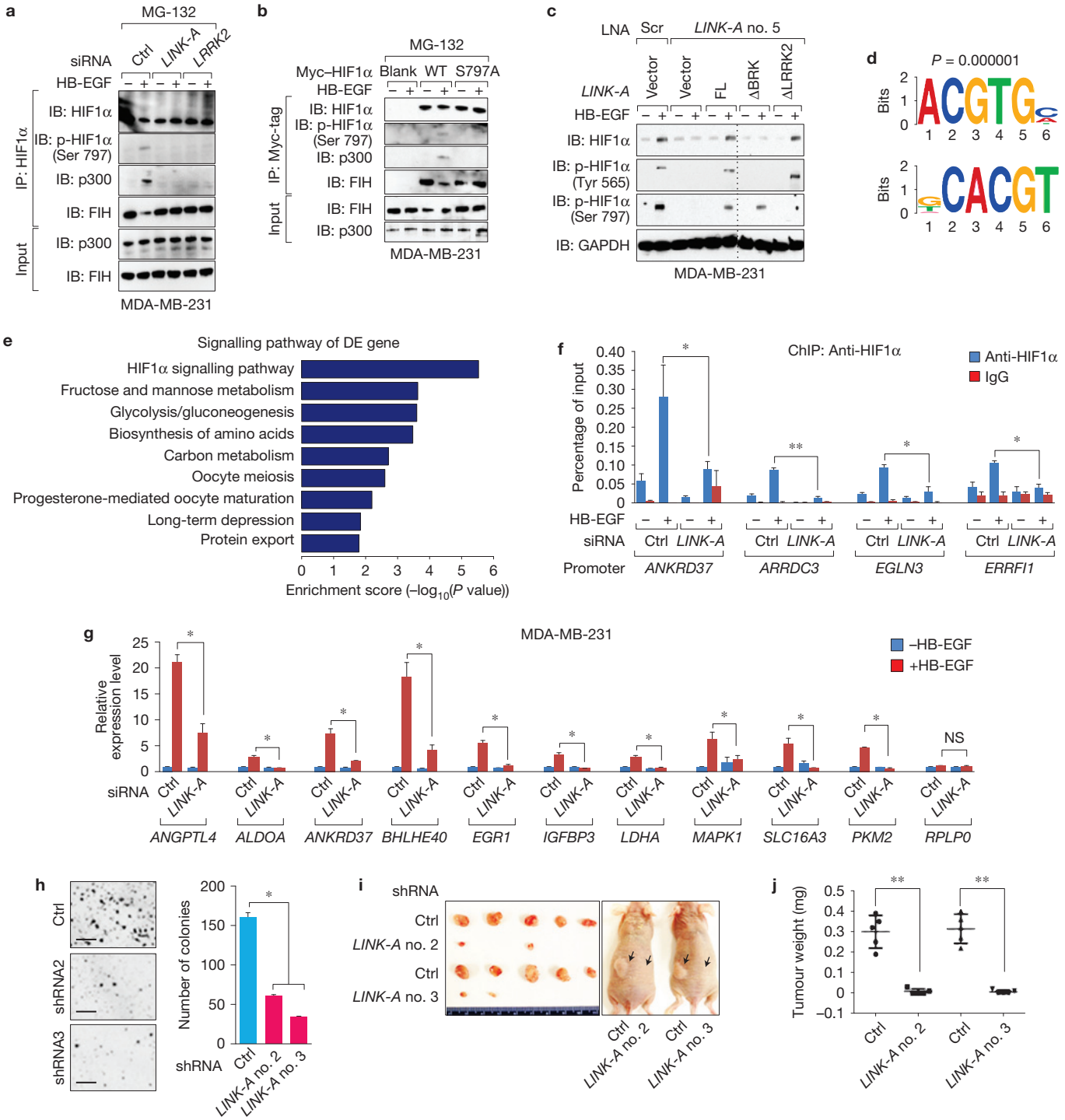

Figure 5 *LINK-A*-recruited LRRK2 phosphorylates HIF1α at Ser 797, enhances HIF1α transcriptional activity and promotes tumour growth. (**a**,**b**) Immunoprecipitation (IP) followed by immunoblot (IB) detection using the indicated antibodies in MDA-MB-231 cells transfected with the indicated siRNAs (**a**) or plasmids (**b**), and treated with MG-132 followed by HB-EGF treatment. (**c**) Immunoblot detection using the indicated antibodies in MDA-MB-231 cells transfected with LNA against *LINK-A* followed by overexpression of the indicated rescue plasmids and HB-EGF stimulation. The dotted line indicates the position where the images of single blots were vertically cropped to juxtapose non-adjacent lanes. (**d**) HIF1α ChIP-seq analysis showing the top enriched HIF-binding consensus motifs. (**e**) HIF1α ChIP-seq analysis showing signalling pathways in MDA-MB-231 cells treated with HB-EGF. (**f**,**g**) ChIP–qPCR detection of HIF1α occupancy on indicated target gene promoters (**f**) and qRT–PCR analysis of HIF1α target genes expression (**g**) in MDA-MB-231 cells transfected with control or *LINK-A* siRNA followed by HB-EGF treatment. (**h**) Colony formation assay in MDA-MB-231 cells transduced with control and *LINK-A* shRNAs. Scale bars, 200 μm. For **f**–**h**, error bars, s.e.m.; $n = 3$ independent experiments ($^{*}P < 0.05$ and $^{**}P < 0.01$, two-tailed paired Student's *t*-test). (**i**,**j**) *In vivo* analyses of tumour growth (**i**) or weight (**j**) in mice that were subcutaneously injected with MDA-MB-231 cells harbouring control or *LINK-A* shRNA. Data are mean ± s.e.m., $n = 5$ mice per group ($^{**}P < 0.01$, two-tailed paired Student's *t*-test). Unprocessed original scans of blots are shown in Supplementary Fig. 7.

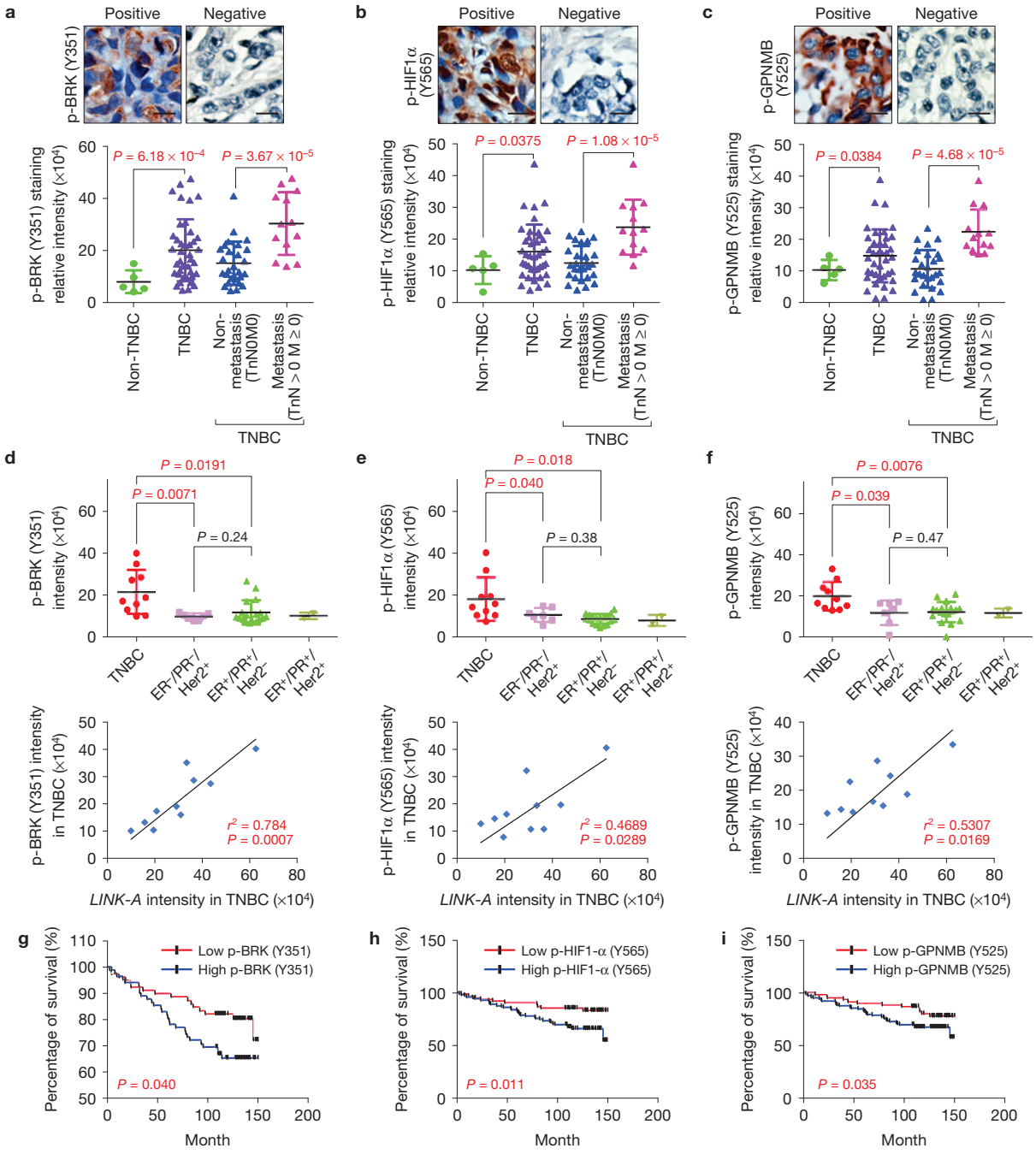

Figure 6 The *LINK-A*-dependent normoxic HIF1α signalling pathway correlates with TNBC. (**a**–**c**) Immunohistochemical staining using antibodies against phospho-BRK (Tyr 351) (**a**), phospho-HIF1α (Tyr 565) (**b**) or phospho-GPNMB (Tyr 525) (**c**) in human breast cancer tissues. Upper panel: representative images (scale bars, 100 μm; lower panel: statistics analysis based on non-TNBC tissues ($n = 5$) versus TNBC tissues ($n = 40$) and non-metastasis (TnN0M0) TNBC ($n = 27$) versus metastasis (TnN > 0 M ≥ 0) breast tissues ($n = 13$) (median, two-way ANOVA). (**d**–**f**) Upper panel: statistical analysis of immunohistochemical staining using antibodies against phospho-BRK (Tyr 351) (**d**), phospho-HIF1α (Tyr 565) (**e**) or phospho-GPNMB (Tyr 525) (**f**) in human breast cancer tissues including TNBC ($n = 10$), ER⁻/PR⁻/HER2⁺ ($n = 7$), ER⁺/PR⁺/HER2⁻ ($n = 18$), and ER⁺/PR⁺/HER2⁺ ($n = 2$) (median, two-way ANOVA). Lower panel: Pearson's correlation analysis comparing staining density between *LINK-A* expression and phospho-BRK (Tyr 351) (**d**), phospho-HIF1α (Tyr 565) (**e**) or phospho-GPNMB (Tyr 525) (**f**) within the TNBC group ($n = 10$ tissue samples, Fisher's exact test). (**g**–**i**) Kaplan–Meier survival analysis of phosphor-BRK (Tyr 351) (**g**), phosphor-HIF1α (Tyr 565) (**h**) and phospho-GPNMB (Tyr 525) (**i**) status in breast cancer patients ($n = 160$, Gehan–Breslow test).

between *LINK-A* expression and the phosphorylation status of BRK, HIF1α and GPNMB in these TNBC tissues (Fig. 6d–f, lower panel), and breast cancer patients with higher levels of these phosphoproteins exhibited a shorter survival time (Fig. 6g–i). Furthermore, the TCGA database revealed that both BRK and LRRK2 are highly expressed in invasive breast carcinoma (Supplementary Fig. 6b). Our data implicate

LINK-A and its associated signalling pathway as potential biomarkers and therapeutic targets for TNBC.

DISCUSSION

Our study reveals that lncRNA directly interacts with non-receptor tyrosine kinase and facilitates its recruitment to the membrane-bound receptor complex and subsequent activation on ligand stimulation, broadening the known mechanisms of lncRNA action (Fig. 6j). The regulatory mechanism of non-receptor tyrosine kinase activation is largely unknown. We propose a model in which *LINK-A* interacts with non-receptor tyrosine kinases to facilitate their activation. At the basal level, BRK, a prototype RNA-binding non-receptor tyrosine kinase, is in a 'closed' conformation and its kinase activity is auto-inhibited, mediated by the self-inhibitory interaction between the SH2 domain and the phospho-C-terminus (Tyr 447; ref. 46). The binding of *LINK-A* to both the SH3 domain and the C-terminal region of BRK leads to a more accessible structure of BRK, which may contribute to higher accessibility by other regulatory proteins and kinases for its activation.

Most common cancer types show increased HIF1α protein levels although hypoxic areas are missing[53,54]. Our study delineates an lncRNA–protein kinase module that regulates normoxic HIF1α stabilization with respect to functional implications in glycolytic reprogramming and tumorigenesis. The *LINK-A*-dependent HIF1α signalling cascade and the consequent effects on cancer cell glycolysis implicate *LINK-A* and *LINK-A*-interacting kinases/receptors as promising therapeutic targets for TNBC. Analyses of the *LINK-A* expression status in the TCGA database and breast cancer tissues both indicated that *LINK-A* significantly correlates with TNBC, revealing an lncRNA that can serve as a biomarker for further classification of TNBC.

Our study identifies four previously unknown phosphorylation sites of GPNMB, BRK and HIF1α in a *LINK-A*-regulated signalling pathway for glycolysis reprogramming in TNBC. These phosphorylation events predict a worse outcome in TNBC patients, suggesting that the *LINK-A*-dependent signalling pathway plays a critical role in TNBC and may provide wide-ranging therapeutic targets for treating TNBC. □

METHODS

Methods and any associated references are available in the online version of the paper.

Note: Supplementary Information is available in the online version of the paper

ACKNOWLEDGEMENTS

We thank S. Kopetz for providing cetuximab and J. Chen for providing SFB-tagged expression vector. We thank D. Aten for assistance with figure presentation. This work was supported by the NIH R00 award (R00DK094981), UT Startup and UT STARS grants to C.Lin, and the NIH R00 award (R00CA166527), CPRIT award (R1218), UT Startup and UT STARS grants to L.Y.

AUTHOR CONTRIBUTIONS

C.Lin, L.Y. and A.L. designed the research, and A.L., C.Li and Z.X. performed most of the experiments, with participation of K.L., S.W., Q.H., Y.Zhang, G.M. and Yubin Z. D.H.H. executed mass spectrometry analysis. Clinical specimens were ascertained and processed by S.W., J.Z., Yan Z. and J.R.M. The histological staining and corresponding analysis were performed by K.L. and Y.W. P.K.P. helped with manuscript preparation. TCGA data and microarray data analysis was performed by C.W., Z.H., L.H. and H.L. M.-C.H. provided reagents and conceptual advice L.Y., C.Lin and A.L. wrote the manuscript.

COMPETING FINANCIAL INTERESTS

The authors declare no competing financial interests.

Published online at http://dx.doi.org/10.1038/ncb3295
Reprints and permissions information is available online at www.nature.com/reprints

1. Cancer Genome Atlas Network. Comprehensive molecular portraits of human breast tumours. *Nature* **490,** 61–70 (2012).
2. Foulkes, W. D., Smith, I. E. & Reis-Filho, J. S. Triple-negative breast cancer. *N. Engl. J. Med.* **363,** 1938–1948 (2010).
3. Hudis, C. A. & Gianni, L. Triple-negative breast cancer: an unmet medical need. *Oncologist* **16,** 1–11 (2011).
4. Prensner, J. R. & Chinnaiyan, A. M. The emergence of lncRNAs in cancer biology. *Cancer Discov.* **1,** 391–407 (2011).
5. Cheetham, S. W., Gruhl, F., Mattick, J. S. & Dinger, M. E. Long noncoding RNAs and the genetics of cancer. *Br. J. Cancer* **108,** 2419–2425 (2013).
6. Gutschner, T. & Diederichs, S. The hallmarks of cancer: a long non-coding RNA point of view. *RNA Biol.* **9,** 703–719 (2012).
7. Lee, J. T. Epigenetic regulation by long noncoding RNAs. *Science* **338,** 1435–1439 (2012).
8. Rinn, J. L. & Chang, H. Y. Genome regulation by long noncoding RNAs. *Annu. Rev. Biochem.* **81,** 145–166 (2012).
9. Batista, P. J. & Chang, H. Y. Long noncoding RNAs: cellular address codes in development and disease. *Cell* **152,** 1298–1307 (2013).
10. Morlando, M., Ballarino, M., Fatica, A. & Bozzoni, I. The role of long noncoding RNAs in the epigenetic control of gene expression. *ChemMedChem* **9,** 505–510 (2014).
11. Orom, U. A., Derrien, T., Guigo, R. & Shiekhattar, R. Long noncoding RNAs as enhancers of gene expression. *Cold Spring Harb. Symp. Quant. Biol.* **75,** 325–331 (2010).
12. Ponting, C. P., Oliver, P. L. & Reik, W. Evolution and functions of long noncoding RNAs. *Cell* **136,** 629–641 (2009).
13. Vance, K. W. & Ponting, C. P. Transcriptional regulatory functions of nuclear long noncoding RNAs. *Trends Genet.* **30,** 348–355 (2014).
14. Wang, X., Song, X., Glass, C. K. & Rosenfeld, M. G. The long arm of long noncoding RNAs: roles as sensors regulating gene transcriptional programs. *Cold Spring Harb. Perspect. Biol.* **3,** a003756 (2011).
15. Yang, L. *et al.* lncRNA-dependent mechanisms of androgen-receptor-regulated gene activation programs. *Nature* **500,** 598–602 (2013).
16. Xing, Z. *et al.* lncRNA directs cooperative epigenetic regulation downstream of chemokine signals. *Cell* **159,** 1110–1125 (2014).
17. Yuan, J. H. *et al.* A long noncoding RNA activated by TGF-β promotes the invasion-metastasis cascade in hepatocellular carcinoma. *Cancer Cell* **25,** 666–681 (2014).
18. Prensner, J. R. *et al.* The long noncoding RNA SChLAP1 promotes aggressive prostate cancer and antagonizes the SWI/SNF complex. *Nat. Genet.* **45,** 1392–1398 (2013).
19. Trimarchi, T. *et al.* Genome-wide mapping and characterization of notch-regulated long noncoding RNAs in acute leukemia. *Cell* **158,** 593–606 (2014).
20. Gupta, R. A. *et al.* Long non-coding RNA HOTAIR reprograms chromatin state to promote cancer metastasis. *Nature* **464,** 1071–1076 (2010).
21. Mercer, T. R. & Mattick, J. S. Structure and function of long noncoding RNAs in epigenetic regulation. *Nat. Struct. Mol. Biol.* **20,** 300–307 (2013).
22. Carrieri, C. *et al.* Long non-coding antisense RNA controls Uchl1 translation through an embedded SINEB2 repeat. *Nature* **491,** 454–457 (2012).
23. Wang, P. *et al.* The STAT3-binding long noncoding RNA lnc-DC controls human dendritic cell differentiation. *Science* **344,** 310–313 (2014).
24. Yoon, J. H., Abdelmohsen, K. & Gorospe, M. Posttranscriptional gene regulation by long noncoding RNA. *J. Mol. Biol.* **425,** 3723–3730 (2013).
25. Castello, A. *et al.* Insights into RNA biology from an atlas of mammalian mRNA-binding proteins. *Cell* **149,** 1393–1406 (2012).
26. Ciesla, J. Metabolic enzymes that bind RNA: yet another level of cellular regulatory network? *Acta Biochim. Pol.* **53,** 11–32 (2006).
27. Lunde, B. M., Moore, C. & Varani, G. RNA-binding proteins: modular design for efficient function. *Nat. Rev. Mol. Cell Biol.* **8,** 479–490 (2007).
28. Semenza, G. L. Targeting HIF-1 for cancer therapy. *Nat. Rev. Cancer* **3,** 721–732 (2003).
29. Denko, N. C. Hypoxia, HIF1 and glucose metabolism in the solid tumour. *Nat. Rev. Cancer* **8,** 705–713 (2008).
30. Wong, C. C. *et al.* Hypoxia-inducible factor 1 is a master regulator of breast cancer metastatic niche formation. *Proc. Natl Acad. Sci. USA* **108,** 16369–16374 (2011).
31. Ivan, M. *et al.* HIFα targeted for VHL-mediated destruction by proline hydroxylation: implications for O_2 sensing. *Science* **292,** 464–468 (2001).
32. Min, J. H. *et al.* Structure of an HIF-1α–pVHL complex: hydroxyproline recognition in signaling. *Science* **296,** 1886–1889 (2002).
33. Knowles, H. J., Mole, D. R., Ratcliffe, P. J. & Harris, A. L. Normoxic stabilization of hypoxia-inducible factor-1α by modulation of the labile iron pool in differentiating U937 macrophages: effect of natural resistance-associated macrophage protein 1. *Cancer Res.* **66,** 2600–2607 (2006).
34. Kuschel, A., Simon, P. & Tug, S. Functional regulation of HIF-1α under normoxia—is there more than post-translational regulation? *J. Cell. Physiol.* **227,** 514–524 (2012).

35. Livasy, C. A. *et al.* Phenotypic evaluation of the basal-like subtype of invasive breast carcinoma. *Mod. Pathol.* **19,** 264–271 (2006).
36. Badve, S. *et al.* Basal-like and triple-negative breast cancers: a critical review with an emphasis on the implications for pathologists and oncologists. *Mod. Pathol.* **24,** 157–167 (2011).
37. Bubb, K. L. *et al.* Scan of human genome reveals no new loci under ancient balancing selection. *Genetics* **173,** 2165–2177 (2006).
38. Regan Anderson, T. M. *et al.* Breast tumor kinase (Brk/PTK6) is a mediator of hypoxia-associated breast cancer progression. *Cancer Res.* **73,** 5810–5820 (2013).
39. Miah, S., Martin, A. & Lukong, K. E. Constitutive activation of breast tumor kinase accelerates cell migration and tumor growth *in vivo*. *Oncogenesis* **1,** e11 (2012).
40. Agalliu, I. *et al.* Higher frequency of certain cancers in LRRK2 G2019S mutation carriers with Parkinson disease: a pooled analysis. *JAMA Neurol.* **72,** 58–65 (2015).
41. Martin, I. *et al.* Ribosomal protein s15 phosphorylation mediates LRRK2 neurodegeneration in Parkinson's disease. *Cell* **157,** 472–485 (2014).
42. Rose, A. A. *et al.* Glycoprotein nonmetastatic B is an independent prognostic indicator of recurrence and a novel therapeutic target in breast cancer. *Clin. Cancer Res.* **16,** 2147–2156 (2010).
43. Ueno, N. T. & Zhang, D. Targeting EGFR in triple negative breast cancer. *J. Cancer* **2,** 324–328 (2011).
44. Maric, G. *et al.* GPNMB cooperates with neuropilin-1 to promote mammary tumor growth and engages integrin $\alpha_5\beta_1$ for efficient breast cancer metastasis. *Oncogene* **34,** 5494–5504 (2015).
45. Saito, Y., Haendeler, J., Hojo, Y., Yamamoto, K. & Berk, B. C. Receptor heterodimerization: essential mechanism for platelet-derived growth factor-induced epidermal growth factor receptor transactivation. *Mol. Cell. Biol.* **21,** 6387–6394 (2001).
46. Qiu, H. & Miller, W. T. Regulation of the nonreceptor tyrosine kinase Brk by autophosphorylation and by autoinhibition. *J. Biol. Chem.* **277,** 34634–34641 (2002).
47. Kamalati, T. *et al.* Brk, a breast tumor-derived non-receptor protein-tyrosine kinase, sensitizes mammary epithelial cells to epidermal growth factor. *J. Biol. Chem.* **271,** 30956–30963 (1996).
48. Brauer, P. M. & Tyner, A. L. Building a better understanding of the intracellular tyrosine kinase PTK6—BRK by BRK. *Biochim. Biophys. Acta* **1806,** 66–73 (2010).
49. Mahon, P. C., Hirota, K. & Semenza, G. L. FIH-1: a novel protein that interacts with HIF-1α and VHL to mediate repression of HIF-1 transcriptional activity. *Genes Dev.* **15,** 2675–2686 (2001).
50. Andrews, S. J. & Rothnagel, J. A. Emerging evidence for functional peptides encoded by short open reading frames. *Nat. Rev. Genet.* **15,** 193–204 (2014).
51. Ruiz-Orera, J., Messeguer, X., Subirana, J. A. & Alba, M. M. Long non-coding RNAs as a source of new peptides. *eLife* **3,** e03523 (2014).
52. Anderson, D. M. *et al.* A micropeptide encoded by a putative long noncoding RNA regulates muscle performance. *Cell* **160,** 595–606 (2015).
53. Stroka, D. M. *et al.* HIF-1 is expressed in normoxic tissue and displays an organ-specific regulation under systemic hypoxia. *FASEB J.* **15,** 2445–2453 (2001).
54. Schwab, L. P. *et al.* Hypoxia-inducible factor 1α promotes primary tumor growth and tumor-initiating cell activity in breast cancer. *Breast Cancer Res.* **14,** R6 (2012).

METHODS

Tissue samples. Breast cancer tissue microarrays were purchased from Biomax, Biochain and USbiolabs. Two sets of fresh frozen breast cancer tissues (Nanjing Cohorts and Duke Cohorts) were obtained from Yixing People's Hospital and Duke University respectively. The study protocol was approved by the Institutional Review Board of Nanjing Medical University and Duke University Health System. All tissue samples were collected in compliance with informed consent policy. Detailed clinical information is summarized in Supplementary Table 1.

Cell culture, transfection and lentiviral transduction. Human breast cancer, human mammary gland epithelia, and human embryonic kidney cell lines were purchased from the American Type Culture Collection (ATCC) and the Characterized Cell Line Core Facility (MD Anderson Cancer Center). siRNA and plasmid transfections were performed using DharmaFECT4 (Thermo Scientific) and Lipofectamine 3000 (Life Technologies). Lentiviruses were produced in HEK293T cells with the ViraPower Lentiviral Expression System. All of the cell lines were free of mycoplasma contamination (tested by the vendors using the MycoAlert kit from Lonza). No cell lines used in this study are found in the database of commonly misidentified cell lines (ICLAC and NCBI Biosample) based on short tandem repeats (STR) profiling performed by vendors.

Cell treatments, crosslinking, fractionation, cell lysis, immunoprecipitation and immunoblotting. Cells were serum starved overnight followed by growth factor (Peprotech) treatment for 30 min at the following concentrations: EGF (10 ng ml^{-1}), amphiregulin (10 ng ml^{-1}), betacellulin (10 ng ml^{-1}), epigen (200 ng ml^{-1}), epiregulin (10 ng ml^{-1}), HB-EGF (10 ng ml^{-1}), heregulin-β1 (5 ng ml^{-1}), TGF-α (2 ng ml^{-1}). Cetuximab (20 μg ml^{-1}) was provided by S. Kopetz (MD Anderson Cancer Center, USA). Chemical crosslinking was carried out as previously described[55] with 1 mM 3,3′-dithiobis(sulphosuccinimidylpropionate) (DTSSP; Pierce). In certain experiments, cells were pre-treated with 10 μM InSolution MG-132 (EMD Millipore) for 6 h before growth factor treatment. Nuclear/cytoplasmic fractionation, cell lysis, immunoprecipitation and immunoblotting were performed as previously described[16].

RNA preparation, northern blot and RACE analysis. RNA *in vitro* transcription and purification were performed as previously described[16]. Total RNAs from 1×10^6 MDA-MB-231 cells with or without HB-EGF treatment were analysed for *LINK-A* and β-actin expression using biotin-labelled LNA probes (Exiqon, sequence are listed in the Oligonucleotide sequences, probes and primers section) according to the NorthernMax Kit (Ambion). RACE–PCR was performed using SMARTer RACE 5′/3′ Kit (Clontech).

Cloning procedures. Full-length *LINK-A* and deletion mutants were constructed by subcloning the gene sequences into pCDNA3.1 (+) backbone (Life Technologies). To generate the LNA no. 5-resistant *LINK-A* mammalian expression vectors used in the rescue experiments, the LNA no. 5 targeting sequence ACA GCT CAT TTA TCC A was mutated to ACA GGC GAT TTA TCC A.

The full-length HIF1α, GPNMB, BRK and LRRK2 mammalian expression vectors were obtained from Origene and Addgene. His-tagged full-length EGFR, extracellular domain (ECD) and intracellular domain (ICD) were provided by M.-C.H. FLAG-tagged full-length GPNMB, ECD + transmembrane domain (TM), and ICD + TM were constructed by subcloning the corresponding gene sequences into an SFB-tagged expression vector (provided by J. Chen, MD Anderson Cancer Center, USA) using the Gateway system (Life Technologies).

Bacterial expression vectors for His-tagged HIF1α and GPNMB ICD were constructed by subcloning the corresponding gene sequences into the pET-DEST42 vector. GST-tagged BRK (WT and mutants) was constructed into the pGEX-5X-1 backbone (GE Healthcare). GST-tagged EGFR ICD, EGFR kinase domain (KD), and EGFR C-terminal domain (CTD) in the pGEX-6p-1backbone were provided by M.-C.H.

All single-point and deletion mutations were generated using the QuikChange Lightning Site-Directed Mutagenesis Kit (Agilent Technologies).

siRNA, shRNA and LNA. Lincode SMARTpool siRNA targeting *LINK-A* (R-027622) and ON-TARGETplus SMARTpool siRNA targeting *EGFR* (L-003114), *GPNMB* (L-011741), *PTK6/BRK* (L-003166) and *LRRK2* (L-006323) from Dharmacon were used in this study. shRNA targeting *LINK-A* was designed on the basis of the Lincode SMARTpool siRNA sequence and cloned into the pLKO.1-Puro vector. LNAs targeting *LINK-A* were designed and synthesized by Exiqon. Detailed sequences are listed in the Oligonucleotide sequences, probes and primers section.

Antibodies. Cell Signaling Technology: anti-EGFR (D38B1) rabbit monoclonal antibody (4267), anti-GPNMB (E1Y7J) rabbit monoclonal antibody (13251), anti-LRRK2 (5559), anti-phospho-EGFR (Tyr845) (D63B4) rabbit monoclonal antibody (6963), anti-phospho-EGFR (Tyr992) (2235), anti-phospho-EGFR (Tyr 1045) (2237), anti-phospho-EGFR (Tyr 1068) (D7A5) rabbit monoclonal antibody (3777), anti-phospho-EGFR (Tyr 1148) (4404), anti-phospho-EGFR (Tyr 1173) (53A5) rabbit monoclonal antibody (4407), anti-hydroxy-HIF1α (Pro 564) (D43B5) rabbit monoclonal antibody (3434), anti-PHD2 (3293), anti-VHL (2738), anti-LRRK2 (5559), anti-EGFR (D38B1) rabbit monoclonal antibody (Alexa Fluor 555 Conjugate) (5108), anti-GST tag (26H1) mouse monoclonal antibody (2624), anti-His-tag (2365) and anti-eIF4B (3592); Santa Cruz Biotechnology: anti-FIH (H-299) (sc-48813), anti-HA (Y-11) (sc-805), anti-BRK (C-18) (sc-1118), anti-GAPDH (6C5) mouse monoclonal antibody (sc-32233) and anti-HIF1α (28b) mouse monoclonal antibody (sc-13515); Millipore: anti-phosphotyrosine (4G10) Platinum mouse monoclonal antibody (05-1050X), anti-Myc tag (4A6) mouse monoclonal antibody (05-724) and anti-eIF4B (ABS281); Thermo Scientific: anti-EGFR (Ab-13) mouse monoclonal antibody (MS-609); Sigma-Aldrich: anti-FLAG tag (M2) mouse monoclonal antibody (F3165); Active Motif: anti-p300 (NM11) mouse monoclonal antibody (61402); Novus Biologicals: anti-HIF1α (NB100-134); Life Technologies: anti-phosphoserine (Poly-Z-PS1); YenZym Antibodies, LLC: anti-phospho-GPNMB (Tyr 525) (p-GPNMB (Tyr 525)), anti-phospho-BRK (Tyr 351) (p-BRK (Tyr 351)), anti-phospho-HIF1α (Tyr 565) (p-HIF1α (Tyr 565)), and anti-phospho-HIF1α (Ser 797) (p-HIF1α (Ser 797)). The specificity of phospho-specific antibodies was confirmed by a blocking peptide competition assay. The antibodies were used as 1:1,000 dilutions for immunoblotting experiments and 1:200 for immunoprecipitation, immunofluorescence and immunohistochemistry experiments.

Protein recombination, purification and *in vitro* translation. Recombinant proteins were expressed in the *Escherichia coli* strain BL21-CodonPlus (DE3)-RIPL (Agilent Technologies) and purified using the Protein Purification Kit (Clontech). Recombinant Flag–GPNMB and PHD1 were purchased from Origene. GST–EGFR was purchased from Active Motif; HIF1α and BRK were purchased from Novus Biologicals. LRRK2 was purchased from SignalChem. Recombinant active caspase-1 was purchased from R&D Systems. *In vitro* translation of *LINK-A* was conducted using TnT Quick Coupled Transcription/Translation Kit and detection was performed using the Transcend Non-Radioactive Translation Detection System (Promega).

RNA pulldown, mass spectrometry analysis, *in vitro* RNA–protein binding assay and *in vitro* RNA–protein binding coupled with dot-blot assay. The cell lysates were freshly prepared using the ProteoPrep Zwitterionic Cell Lysis Kit, Mass Spec Grade (Protea) with Anti-RNase, Protease/Phosphatase Inhibitor Cocktail, Panobinostat and Methylstat supplemented in the lysis buffer. The BcMag Monomer avidin Magnetic Beads (Bioclone) were first prepared according to the manufacturer's instructions and then immediately subjected to RNA (20 μg) capture in RNA capture buffer (20 mM Tris-HCl pH 7.5, 1 M NaCl, 1 mM EDTA) for 30 min at room temperature with agitation. The RNA-captured beads were washed once with NT2 buffer (50 mM Tris-HCl pH 7.4, 150 mM NaCl, 1 mM $MgCl_2$, 0.05% NP-40) and incubated with 30 mg cell lysates diluted in NT2 buffer supplemented with 50 U ml^{-1} Anti-RNase, 2 mM dithiothreitol, 30 mM EDTA and Heparin 0.02 mg ml^{-1} for 4 h at 4 °C with rotation. The RNA-binding protein complexes were washed sequentially with NT2 buffer (twice), NT2-high-salt buffer containing 500 mM NaCl (twice), NT2-high-salt buffer containing 1 M NaCl (once), NT2-KSCN buffer containing 750 mM KSCN (twice) and PBS (once) for 5 min at 4 °C and eluted by 2 mM D-biotin in PBS. The eluted protein complexes were denatured, reduced, alkylated and digested with immobilized trypsin (Promega) for MS analysis at MD Anderson Cancer Center Proteomics Facility. The RNA–protein binding assays and *in vitro* RNA–protein binding coupled with dot-blot assay were performed as described previously[16].

RNAScope assay, RNA FISH, immunofluorescence and immunohistochemistry. RNAScope assay and RNA FISH were performed as previously described[16]. RNAScope probes targeting *LINK-A* (Cat. no. 412027), *BCAR4* (Cat. no. 407777) or *HOTAIR* (Cat. no. 312347) were custom designed or purchased from Advanced Cell Diagnostics. LNA FISH probes targeting *LINK-A* and a control probe targeting β-actin (300512-04) were purchased from Exiqon (sequences are listed in the Oligonucleotide sequences, probes and primers section).

For immuno-RNA FISH, the slide from RNA FISH was further blocked with blocking buffer (1 × PBS, 5% BSA, 0.3% Triton X-100) for 1 h at room temperature followed by incubation with primary antibodies (diluted 1:200) for 1 h at room temperature. After incubation with fluorochrome-conjugated secondary antibodies for 1 h at room temperature in the dark, the slide was washed and mounted for detection. Immunofluorescence and immunohistochemistry were performed as previously described[16].

The quantification of RNAScope staining densities was measured by RNAscope SpotStudio v1.0 Software (Advanced Cell Diagnostics). The quantification of IHC

DOI: 10.1038/ncb3295

staining density was performed by Image-Pro plus 6.0 (Media Cybernetics) and calculated on the basis of the average staining intensity and the percentage of positively stained cells.

Computational analysis of TCGA RNA-Seq data. Breast cancer RNA-seq BAM files was downloaded from UCSC Cancer Genomics Hub (CGHub, https://cghub.ucsc.edu). TCGA BAM files were generated based on the MapSplice algorithm for alignment against the hg19 reference genome using default parameters[56]. We then quantified lncRNA expression of *LINK-A* as RPKM (reads per kilobase per million mapped reads[57]) as previously described[58], and the analysis was based on $\log_2$(RPKM+1). Clinical information, PAM50 subtype, and ER, PR and HER2 status were obtained from the TCGA marker paper[1]. We used analysis of variance (ANOVA) or Student's *t*-test to detect the statistical difference between two or more groups.

***In vitro* kinase assay.** Wild-type or mutant substrate proteins were incubated with 50 μl of *in vitro* kinase assay buffer II (SignalChem) containing 100 μM ATP (cold reaction) or 10 μCi [γ-^{32}P]ATP and the indicated protein kinase for 1 h at 30 °C. Resulting products were separated by SDS–PAGE and detected by Coomassie blue staining, autoradiography or immunoblotting with phospho-specific antibodies. The specific BRK and LRRK2 kinase activities were measured using a Universal Kinase Activity Kit (R&D Systems).

***In vitro* HIF1α hydroxylation assay.** Five micrograms of wild-type His-tagged HIF1α or the Y565F mutant was incubated with 1 μg recombinant PHD1 in a reaction buffer containing 10 μM $FeSO_4$, 100 μM 2-oxo-glutarate, 1 mM ascorbate, 100 μM dithiothreitol, and 50 μM Tris-HCl (pH 7.8) at 37 °C for 1 h. HIF1α hydroxylation was analysed by SDS–PAGE and immunoblotting with specific antibody against Pro 564 hydroxylation. For the quantitative peptide hydroxylation assay, 10 μg synthesized unmodified peptide (LDLEMLAPYI) or Tyr-565-phosphopeptide (LDLEMLAP-pY-I) and 3 μg recombinant PHD1 were incubated in the same reaction buffer described above or in the same buffer, except containing 100 μM DMOG. Resulting peptides were purified by ZipTip and analysed by liquid chromatography coupled with tandem MS (LC–MS) to confirm the presence of the proline-hydroxylated peptides. The acquired MS/MS data were searched against a database to identify hydroxylated proline sites through a dynamic mass shift for the modified proline (+15.9949 Da).

Chromatin immunoprecipitation (ChIP), RNA immunoprecipitation (RIP), ChIP-seq and data analysis. ChIP and RIP were performed as previously described[16]. ChIP-seq and data analysis were performed by ArrayStar. The mapped reads were used for peak detection by MACS v1.4.0 (Model-based Analysis of ChIP-Seq) software. Statistically significant ChIP-enriched regions (peaks) were identified by comparison to a Poisson background model (Cutoff *P* value = 10^{-4}).

Anchorage-independent growth assay, glucose uptake assay and lactate production assay. The anchorage-independent growth assay was performed as previously described[59]. Glucose uptake and lactate production assays were performed using the Glucose Uptake Cell-based Assay Kit and the L-Lactate Assay Kit (Cayman Chemical) respectively. Lactate production was expressed as lactate concentration per 10^4 viable cells.

***In vivo* tumorigenesis study.** All animal experiments were performed in accordance with a protocol approved by the Institutional Animal Care and Use Committee of MD Anderson Cancer Center. Animals arriving in our facility were randomly put into cages with five mice each. They were implanted with respective tumour cells in the unit of cages, which were randomly selected. The animal experiment was set up to use 5 mice per group to detect a twofold difference with power of 80% and at the significance level of 0.05 by a two-sided test for significant studies. Tumour cells in 30 μl growth medium (mixed with Matrigel at a 1/1 ratio) were injected subcutaneously into the flank of six- to eight-week-old female nude mice. Tumour size was measured every five days using a calliper, and tumour volume was calculated using the standard formula: $0.54 \times L \times W^2$, where L is the longest diameter and W is the shortest diameter. The tumours were removed, photographed and weighed. The investigators were not blinded to allocation during experiments and outcome assessment.

Oligonucleotide sequences (5′–3′), probes (5′–3′) and primers (forward and reverse). qPCR primers for gene expression and RIP: *LINK-A* (5′-TTC CCC CA T TTT TCC TTT TC-3′ and 5′-CTC TGG TTG GGT GAC TGG TT-3′); *GAPDH* (5′-GAA GGT GAA GGT CGG AGT-3′ and 5′-GAA GAT GGT GAT GGG ATT TC-3′); *ANGPTL4* (5′-CAC AGC CTG CAG ACA CAA CT-3′ and 5′-AAA CTG GCT TTG CAG ATG CT-3′); *ALDOA* (5′-CTG CCA GTA TGT GAC CGA GA-3′ and 5′-ACA GGA AGG TGA TCC CAG TG-3′); *ANKRD37* (5′-GTA GCC AGT GAT GCC CAA AT-3′ and 5′-CTT CCG AGA CTC CGT TTC TG-3′); *BHLHE40* (5′-CCT TGA AGC ATG TGA AAG CA-3′ and 5′-GCT TGG CCA GAT ACT GAA GC-3′); *EGR1* (5′-TGA CCG CAG AGT CTT TTC CT-3′ and 5′-TGG GTT GGT CAT GCT CAC TA-3′); *IGFBP3* (5′-GGG GTG TAC ACA TTC CCA AC-3′ and 5′-AGG CTG CCC ATA CTT ATC CA-3′); *LDHA* (5′-TGT GCC TGT ATG GA G TGG AA-3′ and 5′-AGC ACT CTC AAC CAC CTG CT-3′); *MAPK1* (5′-CCA G AG AAC CCT GAG GGA GA-3′ and 5′-TCG ATG GTT GGT GCT CGA AT-3′); *PKM2* (5′-ATC GTC CTC ACC AAG TCT GG-3′ and 5′-GAA GAT GCC ACG G TA CAG GT-3′); *RPLP0* (5′-TGG TCA TCC AGC AGG TGT TCG A-3′ and 5′-AC A GAC ACT GGC AAC ATT GCG G-3′); *HIF1α* (5′-GTC TGA GGG GAC AGG AGG AT-3′ and 5′-CTC CTC AGG TGG CTT GTC AG-3′); *B2M* (5′-GGC TAT C CA GCG TAC TCC AA-3′ and 5′-TGG ATG AAA CCC AGA CAC ATA-3′).

qPCR primers for *LINK-A* knockdown-rescue gene expression and RIP experiments: *LINK-A* (5′-TAT GGA GGA TCG CTG TTT CC-3′ and 5′-CCA AAG ATG TCG CAG GAC TT-3′).

siRNA sequences: *LINK-A* (5′-UGU CUA AGG UGG AGA UUA C-3′, 5′-AGA UGU AGU UCU AGU UCA U-3′, 5′-UUA CUG AGG UUG AAU AUG U-3′ and 5′-GGU CUU CAU UCU UAC GCU U-3′); *EGFR* (5′-CAA AGU GUG UAA CG G AAU A-3′, 5′-CCA UAA AUG CUA CGA AUA U-3′, 5′-GUA ACA AGC UCA CGC AGU U-3′, and 5′-CAG AGG AUG UUC AAU AAC U-3′); *GPNMB* (5′-GG A AUU UCA UCU ACG UCU U-3′, 5′-AUA UAA CAU UUG CGG UGA A-3′, 5′-UGC AAG AAG AGG CGG GAU A-3′, and 5′-CCA GAA GAA CGA UCG AAA U-3′); *PTK6/BRK* (5′-GAG AAA GUC CUG CCC GUU U-3′, 5′-CCA UUA AGG UGA UUU CUC G-3′, 5′-UGC CCG AGC UUG UGA ACU A-3′, and 5′-GGC CA U UAC UCC ACC AAA U-3′); *LRRK2* (5′-CAA GUU AUU UCA AGG CAA A-3′, 5′-UUA CCG AGA UGC CGU AUU A-3′, 5′-GGA GGG AUC UUC UUU AAU U -3′, and 5′-GAA AUU AUC AUC CGA CUA U-3′).

LNA GapmeR sequences: Negative control (5′-AAC ACG TCT ATA CGC-3′); *LINK-A* no. 1 (5′-GCG TAA GAA TGA AGA-3′); *LINK-A* no. 2 (5′-GTG ATA A GA CTA AGT G-3′); *LINK-A* no. 3(5′-GAA TAA GGA TAA GCG T-3′); *LINK-A* no. 4 (5′-CCA CAG CTT GAA TTC C-3′) and *LINK-A* no. 5 (5′-TGG ATA AAT G AG CTG T-3′).

LINK-A shRNA sequences: *LINK-A* shRNA1 (5′-TGT CTA AGG TGG AGA TTA C-3′); *LINK-A* shRNA2 (5′-AGA TGT AGT TCT AGT TCA T-3′); *LINK-A* shRNA3 (5′-TTA CTG AGG TTG AAT ATG T-3′); *LINK-A* shRNA4 (5′-GGT CT T CAT TCT TAC GCT T-3′).

RNA FISH probes: *LINK-A* (/56-FAM/TGT 5′-AGC CAC AGA CAT CAT TA C A-3′), β-actin (/Fluorescein/5′-CTC ATT GTA GAA GGT GTG GTG CCA-3′).

LNA RNA detection probes: β-actin (/5Biosg/5′-CTC ATT GTA GAA GGT GTG GTG CCA-3′) and *LINK-A* (/5Biosg/5′-ACT AAG TGT TGG CAG GTT ATG T-3′).

LINK-A RACE–PCR primers: 3′-RACE (TGG AAT TCA AGC TGT GGG TG) and 5′-RACE (GCA TTT TTA TTT TAA TTG AGG).

qPCR primers for ChIP: EGLN3 (5′-CGT GGA GGA CTG GCT CTA AG-3′ and 5′-GGT GTG CTC GGG TGT G-3′; ref. 60), ERRFI1 (5′-GAT TAC AGG CTG GAT GGC AC-3′ and 5′-TGC TGC CAG ACT GGT ATG AG-3′; ref. 61), ARRDC3 (5′-CCC CTG CAG TCA CAC ACT C-3′ and 5′-TTT GTC ACA TGG GAC TCT TC-3′; ref. 31), ANKRD37 (5′-CCA GTT TCC TGG TTA CGT GC-3′ and 5′-TAA GTC AGT GGG CGT GAG AG-3′; ref. 62), RPLP0 (5′-TGA AGA GCA GAG GCG ACC CAC-3′ and 5′-ATG GGT GTC GGC GTG AC-3′; ref. 60).

Statistics and reproducibility. The experiment was set up to use 3–5 samples/repeats per experiment/group/condition to detect a twofold difference with power of 80% and at the significance level of 0.05 by a two-sided test for significant studies. For RNAscope, immunostaining, immunohistochemical staining, colony formation assay, northern blotting, RACE analysis, and western blotting, representative images are shown. Each of these experiments was independently repeated 3–5 times. Relative quantities of gene expression level were normalized to *B2M*. The relative quantities of ChIP samples were normalized by individual inputs, respectively. Results are reported as mean ± standard error of the mean (s.e.m.) of at least three independent experiments. Each exact *n* values are indicated in the corresponding figure legend. Comparisons were performed using two-tailed paired Student's *t*-test or two-way ANOVA ($^*P < 0.05$, $^{**}P < 0.01$, and $^{***}P < 0.001$), as indicated in the individual figures. Fisher's exact test was implemented for statistical analyses of the correlation between markers and clinical parameters. For survival analysis, the expression of *LINK-A* or phosphorylation density of indicated proteins was treated as a binary variant and divided into 'high' and 'low' level. Kaplan–Meier survival curves were compared using the Gehan–Breslow test with GraphPad Prism (GraphPad Software). The experiments were not randomized. The investigators were not blinded to allocation during experiments and outcome assessment.

55. Yu, X., Sharma, K. D., Takahashi, T., Iwamoto, R. & Mekada, E. Ligand-independent dimer formation of epidermal growth factor receptor (EGFR) is a step separable from ligand-induced EGFR signaling. *Mol. Biol. Cell* **13,** 2547–2557 (2002).

56. Wang, K. *et al.* MapSplice: accurate mapping of RNA-seq reads for splice junction discovery. *Nucleic Acids Res.* **38,** e178 (2010).
57. Mortazavi, A., Williams, B. A., McCue, K., Schaeffer, L. & Wold, B. Mapping and quantifying mammalian transcriptomes by RNA-Seq. *Nat. Methods* **5,** 621–628 (2008).
58. Han, L. *et al.* The Pan-Cancer analysis of pseudogene expression reveals biologically and clinically relevant tumour subtypes. *Nat. Commun.* **5,** 3963 (2014).
59. Borowicz, S. *et al.* The soft agar colony formation assay. *J. Vis. Exp.* **92,** e51998 (2014).
60. Ortiz-Barahona, A., Villar, D., Pescador, N., Amigo, J. & del Peso, L. Genome-wide identification of hypoxia-inducible factor binding sites and target genes by a probabilistic model integrating transcription-profiling data and *in silico* binding site prediction. *Nucleic Acids Res.* **38,** 2332–2345 (2010).
61. Schodel, J. *et al.* High-resolution genome-wide mapping of HIF-binding sites by ChIP-seq. *Blood* **117,** e207–e217 (2011).
62. Benita, Y. *et al.* An integrative genomics approach identifies hypoxia inducible factor-1 (HIF-1)-target genes that form the core response to hypoxia. *Nucleic Acids Res.* **37,** 4587–4602 (2009).

This Supplementary Information file was updated with correct captions for Supplementary Figures 3–5 on 10 February 2016.

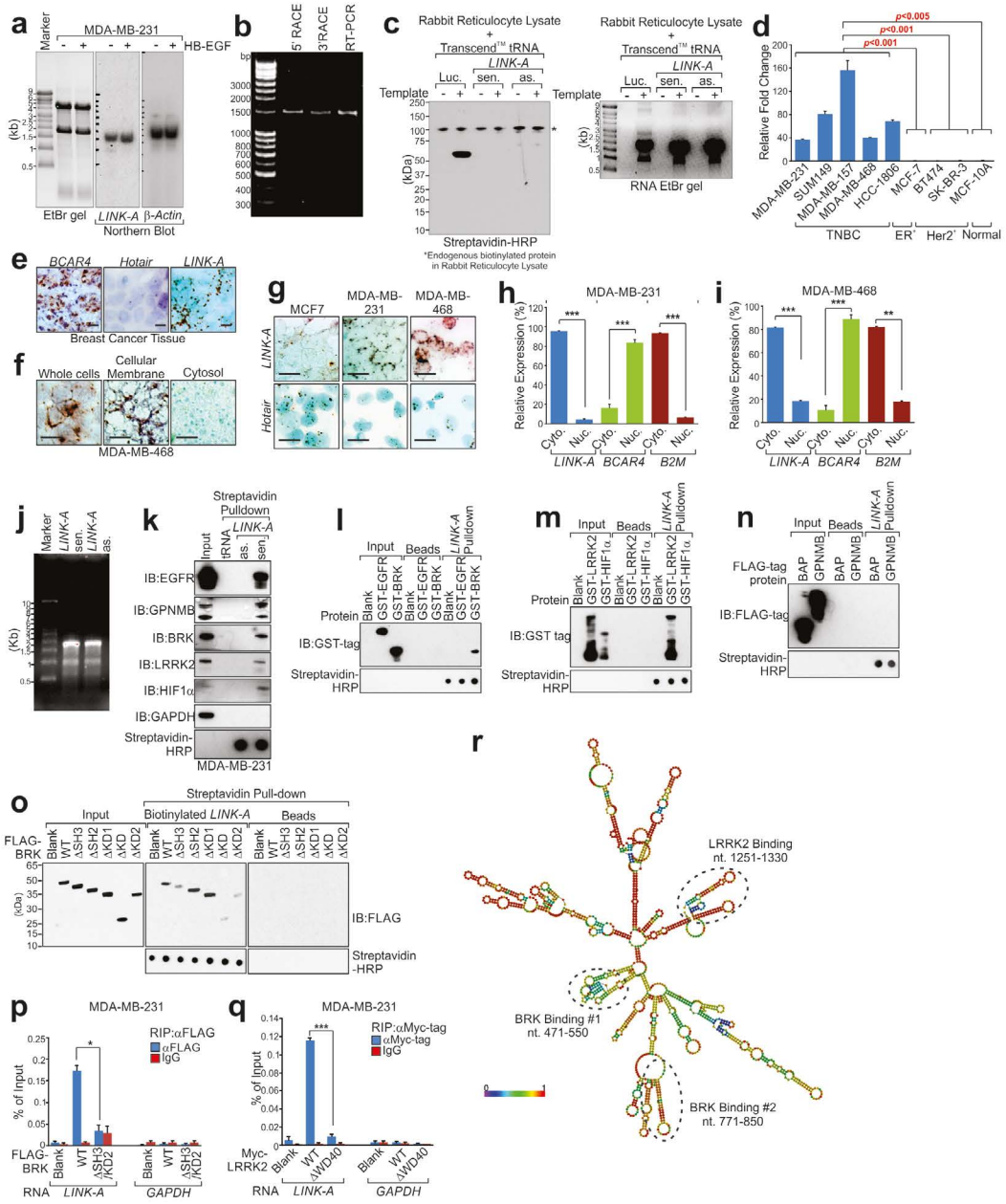

Supplementary Figure 1 Characterization of *LINK-A* protein-coding potential, subcellular localization, and *LINK-A*-protein interactions. **(a)** Northern blot detection of *Beta-Actin* and *LINK-A* in MDA-MB-231 cells with indicated treatment. (**b**) 5' and 3' RACE-PCR of *LINK-A* in MDA-MB-231 cells. (**c**) *In vitro* translation of *LINK-A* sense or antisense transcript. *Luciferase* (*Luc*) is used as a positive control. Endogenous biotinylated protein in rabbit reticulocyte lysate was indicated with an asterisk. (**d**) qRT-PCR analyses of *LINK-A* expression level in various breast normal and cancer cell lines. (**e** and **f**) RNAScope® analysis of the indicated lncRNAs in breast cancer tissues (e) or indicated breast cancer cell lines (f). Scale bars, 100μm. (**g**) RNAScope® detection of plasma membrane localization of *LINK-A* in MDA-MB-468 cell fractionations. Scale bars, 100μm. (**h** and **i**) Cytoplasmic and nuclear RNA were fractionated and detected by qPCR. *GAPDH* and *BCAR4* were used as cytoplasmic and nuclear markers respectively. (**j**) Denaturing agarose gel electrophoresis of *in vitro* transcribed biotinylated *LINK-A* sense and antisense transcripts. **(k-n)** RNA pulldown followed by IB detection of proteins retrieved by *in vitro* transcribed biotinylated *LINK-A* from MDA-MB-231 cell lysates (k) or from recombinant proteins (l-n). Streptavidin-HRP indicated the presence of equal amount of biotinylated RNA transcripts (l-n). **(o)** Streptavidin pulldown followed by IB detection using biotinylated *LINK-A* and cell lysates extracted from MDA-MB-231 cells transfected with indicated expression vectors. Streptavidin-HRP indicated the presence of equal amount of biotinylated RNA transcripts. (**p** and **q**) RIP-qPCR detection of indicated RNAs retrieved by FLAG-tag (p) or Myc-tag (q) in MDA-MB-231 cells transfected with indicated expression vectors. **(r)** Graphic illustration of predicted *LINK-A* secondary structure and the binding sites of *LINK-A* corresponding to BRK and LRRK2 binding. For panels **d**, **h**, **i**, **p**, **q**, error bars, S.E.M., n=3 independent experiments (*p<0.05, **p<0.01 and ***p<0.001, two-tailed paired Student's t-test).

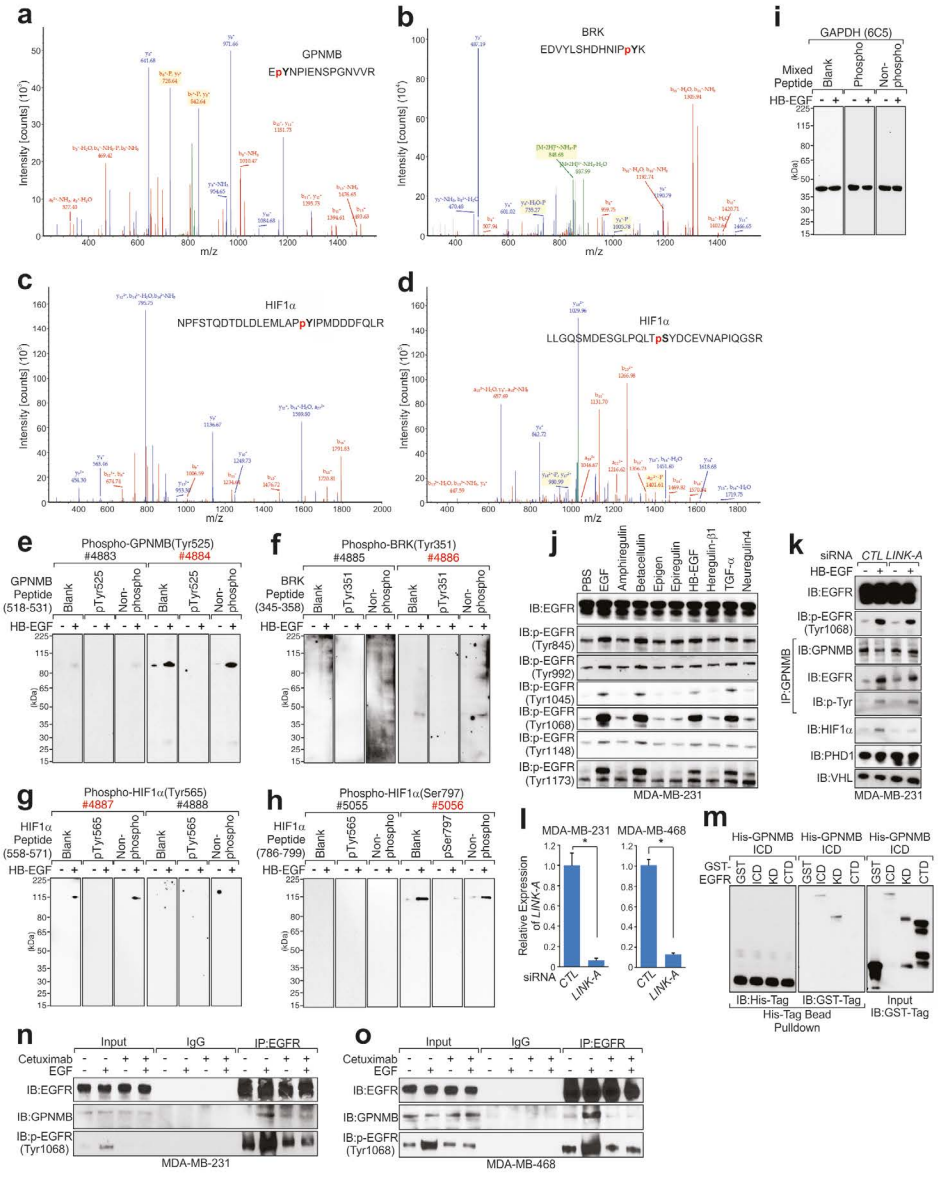

Supplementary Figure 2 Characterization of HB-EGF-induced phosphorylation of GPNMB, BRK and HIF1α and domain mapping of EGFR-GPNMB interaction. (**a**) Annotated MS/MS spectrum assigned to GPNMB peptide sequence: EYNPIENSPGNVVR, Y2-Phospho (79.96633 Da) double charge, monoisotopic m/z: 834.37469 Da (-0.22 mmu/-0.26 ppm), MH+: 1667.74211 Da, RT: 2.88 min, mascot (v1.30); ionScore:58, exp value:4.7E-004. (**b**) Annotated MS/MS spectrum assigned to BRK peptide sequence: EDVYLSHDHNIPYK, Y13-Phospho (79.96633 Da) double charge, monoisotopic m/z: 905.39587 Da (+0.04 mmu/+0.04 ppm), MH+: 1809.78447 Da, RT: 1.97 min, identified with: Mascot (v1.30); ionScore:35, exp value:9.9E-002. (**c**) Annotated MS/MS spectrum assigned to HIF1α peptide sequence: NPFSTQDTDLDLEMLAPYIPMDDDFQLR, Y18-Phospho (79.96633 Da), charge: +3, monoisotopic m/z: 1127.49597 Da (-0.22 mmu/-0.19 ppm), MH+: 3380.47336 Da, RT: 29.88 min, identified with: Mascot (v1.30); ionScore:55, exp value:2.5E-003. (**d**) Annotated MS/MS spectrum assigned to HIF1α peptide sequence: LLGQSMDESGLPQLTSYDCEVNAPIQGSR, S16-Phospho (79.96633 Da), charge: +3, monoisotopic m/z: 1063.48022 Da (-0.53 mmu/-0.5 ppm), MH+: 3188.42612 Da, RT: 18.35 min, identified with: mascot (v1.30); ionScore:50, exp value:8.2E-003. Data were acquired from analysis of the tryptic digest by high-sensitivity LCMS/MS on an Orbitrap Elite high-resolution mass spectrometer. (**e-i**) IB detection of phospho-GPNMB (Tyr525) (e), phospho-BRK (Tyr351) (f), phospho-HIF1α (Tyr565) (g), phospho-HIF1α (Ser797) (h), and GAPDH (i) in lysates extracted from MDA-MB-231 cells treated with or without HB-EGF using antibodies pre-incubated with indicated blocking peptides. Antibodies generated from two independent rabbits were tested and the highlighted (red) one was used in this study. (**j**) IB detection using indicated antibodies in MDA-MB-231 cells treated with indicated ligands. (**k**) IP followed by IB detection using indicated antibodies in MDA-MB-231 cells transfected with indicated siRNAs followed by HB-EGF treatment. (**l**) qRT-PCR analyses of *LINK-A* expression level in MDA-MB-231(left panel) and in MDA-MB-468 (right panel) cells transfected with control siRNA or *LINK-A* siRNA smart pool. Error bars, S.E.M., n=3 independent experiments (*p<0.05, two-tailed paired Student's t-test). (**m**) His-tag pulldown followed by IB detection using His-tagged GPNMB intracellular domain (ICD) and GST-tagged EGFR intracellular domain (ICD), kinase domain (KD), C-terminal domain (CTD). (**n** and **o**) IP followed by IB detection using indicated antibodies in MDA-MB-231 and MDA-MB-468 cells transfected with indicated siRNAs treated with Cetuximab (20 μg/ml) for 4 hours followed by HB-EGF treatment for 30 minutes.

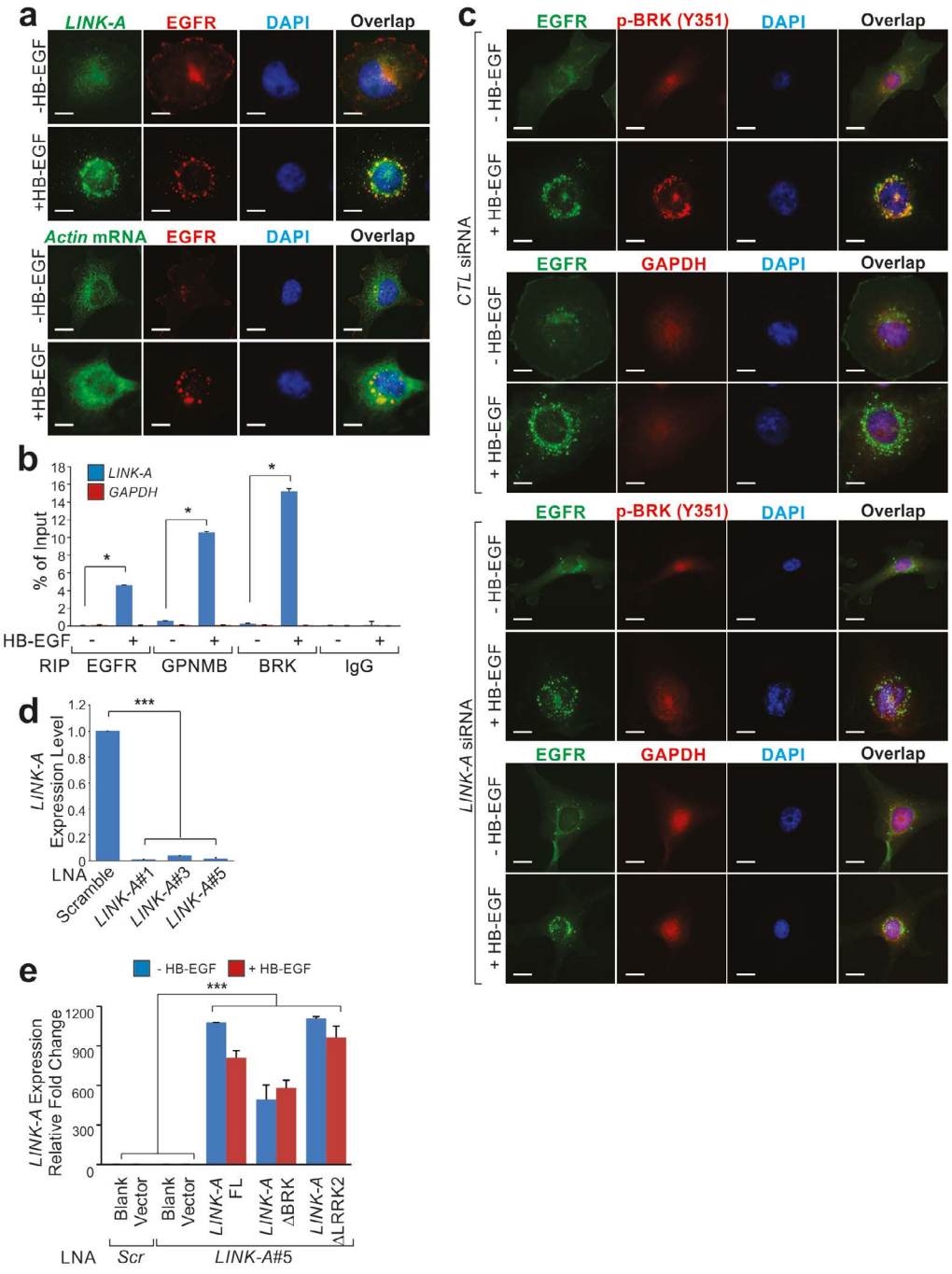

Supplementary Figure 3 Characterization of HB-EGF-triggered, *LINK-A*-dependent BRK recruitment and activation. **(a)** Immuno-RNA FISH assay using RNA FISH probes against *LINK-A* (upper panel) or *Actin* mRNA (lower panel) and antibody against EGFR in MDA-MB-231 cells treated with HB-EGF. Scale bars, 20μm. **(b)** RIP-qPCR detection of indicated RNAs retrieved by EGFR-, GPNMB- or BRK- specific antibodies in MDA-MB-231 cells treated with or without HB-EGF. (**c**) Immunofluorescence imaging using antibodies as indicated in MDA-MB-231 cells harboring control (left panel) or *LINK-A* shRNA (right panel) followed by HB-EGF stimulation. Scale bars, 20μm. **(d)** qRT-PCR analyses of *LINK-A* expression level in MDA-MB-231 cells transfected with indicated LNAs. **(e)** qRT-PCR analysis of *LINK-A* expression level in MDA-MB-231 cells transfected with LNA against *LINK-A* followed by overexpression of indicated rescue plasmids and HB-EGF treatment. For panels **b**, **d**, **e**, error bars, S.E.M., n=3 independent experiments (*p<0.05 and ***p<0.001, two-tailed paired Student's t-test).

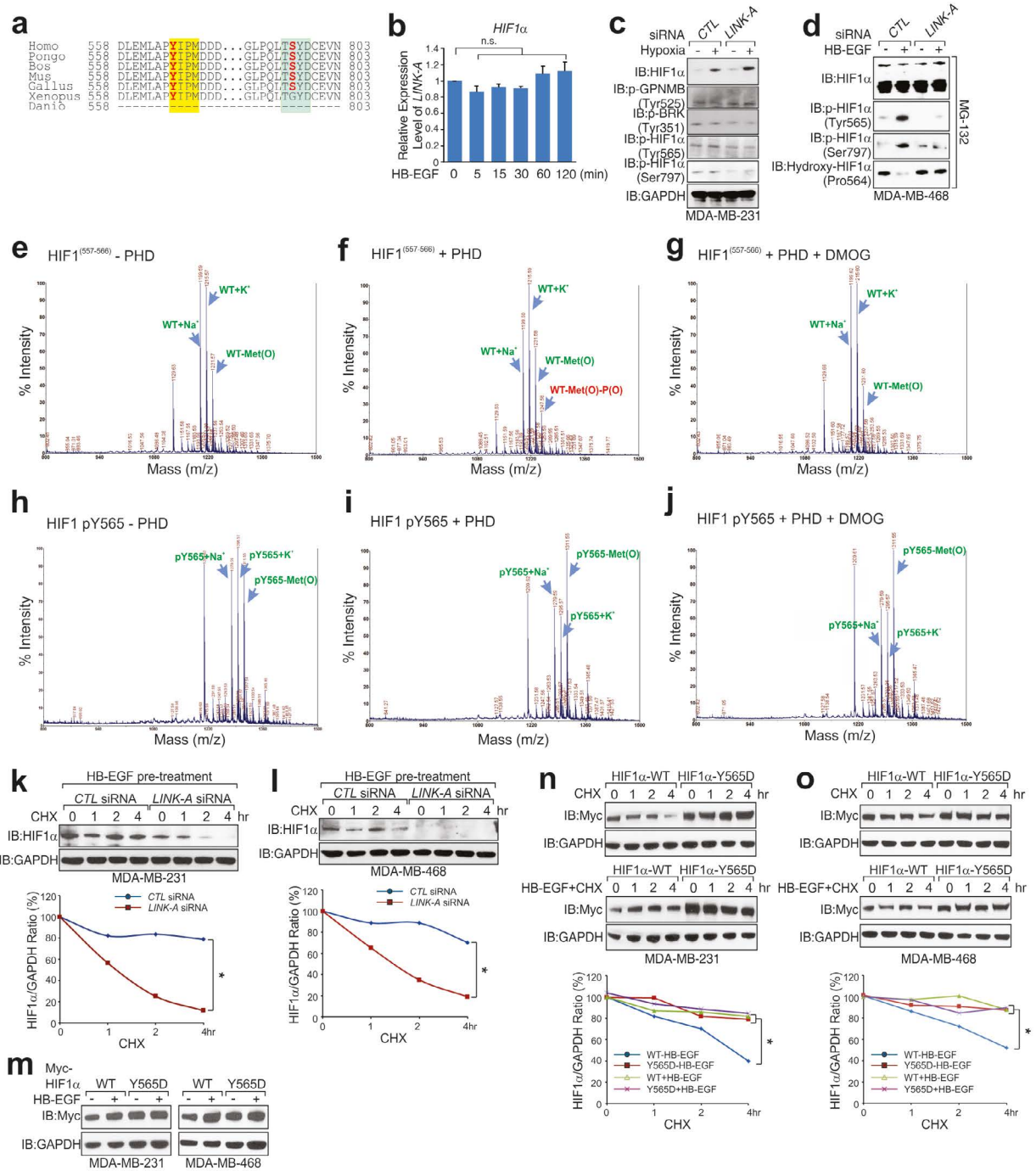

Supplementary Figure 4 Examination of *LINK-A*-regulated HIF1α Tyr565 phosphorylation, Pro564 hydroxylation and protein half-life. (**a**) Conservation of HIF1α pYXXM motif containing phosphorylated tyrosine between species. (**b**) qRT-PCR analysis of HIF1α expression level in MDA-MB-231 cells treated with HB-EGF at indicated time points. Error bars, S.E.M. of three independent experiments Error bars, S.E.M., *n*=3 independent experiments (n.s., *p*>0.05, two-tailed paired Student's *t*-test). (**c**) IB detection of indicated phospho-proteins in MDA-MB-231 cells transfected with control or *LINK-A* siRNA followed by hypoxia treatment for 4 hours. (**d**) IB detection using indicated antibodies in MDA-MB-468 cells transfected with control or *LINK-A* siRNAs followed by MG-132 and further HB-EGF treatment. (**e-j**) *In vitro* hydroxylation assay with unphosphorylated (e-g) or Tyr565 phosphorylated (h-j) HIF1α peptide showing the PHD1-dependent HIF1α hydroxylation at Pro564 in the absence or presence of the PHD inhibitor, DMOG. The resultant peptides were subjected to LC-MS analysis. The peptides with correspondent modifications were shown. (**k** and **l**) Upper panel: IB detection using indicated antibodies in MDA-MB-231(k) or MDA-MB-468 (l) cells transfected with control or *LINK-A* siRNAs followed by HB-EGF and cycloheximide (CHX, 100 μg/ml) treatment at indicated time point. Lower panel: quantification of HIF1α protein levels in k and l. (**m**) IB detection using indicated antibodies in MDA-MB-231 (left panel) or MDA-MB-468 (right panel) cells transfected with Myc-HIF1α WT or mutant followed by HB-EGF treatment. (**n** and **o**) Upper and middle panel: IB detection using indicated antibodies in MDA-MB-231(n) or MDA-MB-468 (o) cells transfected with Myc-HIF1α WT or mutants followed by no treatment (upper panel) or HB-EGF treatment (middle panel) and further cycloheximide (CHX, 100 μg/ml) treatment at indicated time point. Lower panel: quantification of HIF1α protein levels in n and o. For panels **k**, **l**, **n** and **o**, error bars, S.E.M., *n*=3 independent experiments (*$p<0.05$, two-tailed paired Student's *t*-test).

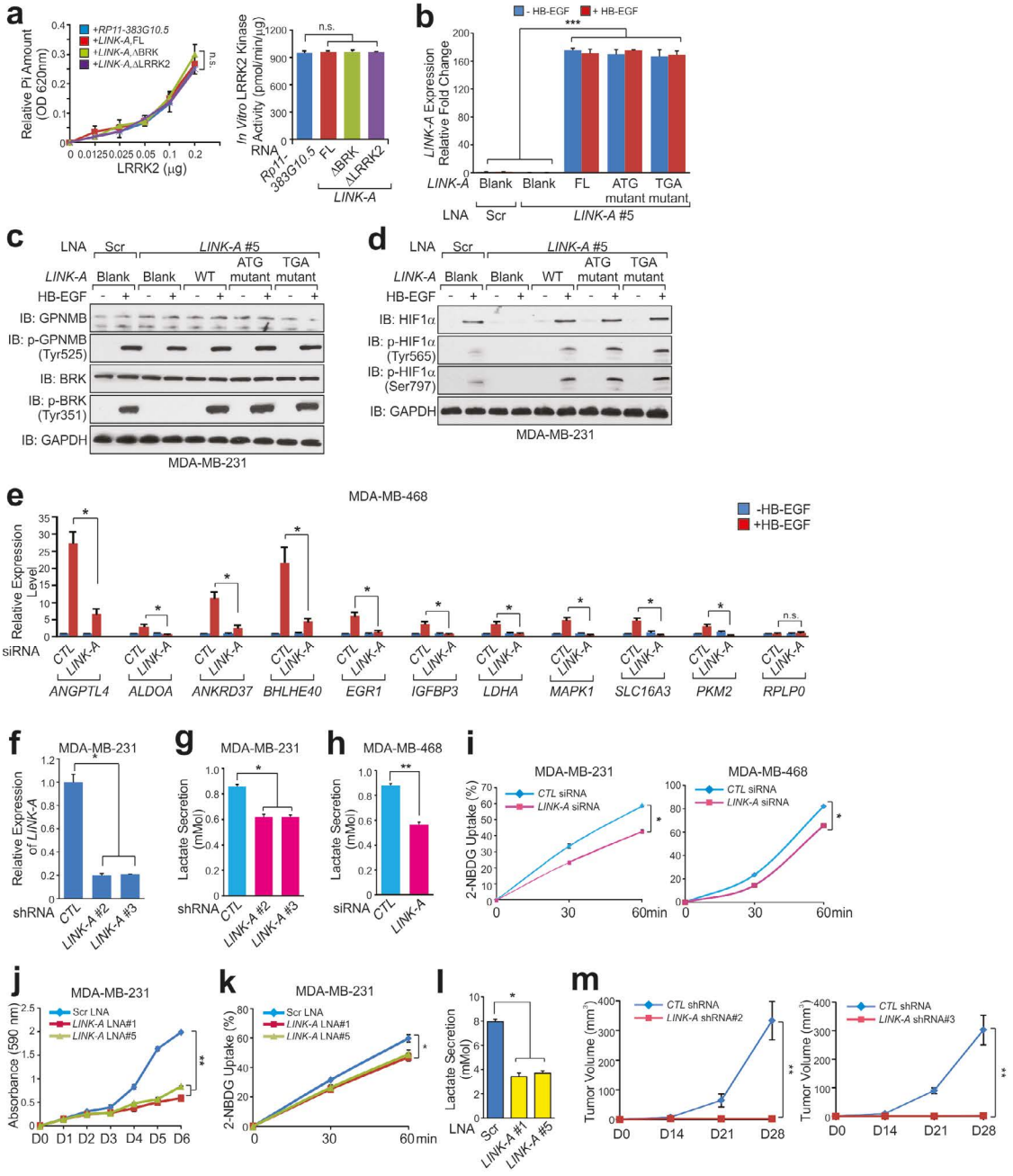

Supplementary Figure 5 *LINK-A* enhances HIF1α transcriptional activity, breast cancer cell glucose metabolism, and tumor growth *in vivo*. (**a**) Quantitative detection of LRRK2 kinase activity in the absence or presence of *LINK-A* or indicated deletion transcripts. Left panel: Relative Pi release monitored by OD 620 nm. Right panel: calculated specific kinase activity (pmol/min/μg) based on Pi measurement. (**b**) qRT-PCR detection of exogenous expressed *LINK-A* wild-type, ATG or TGA mutants. (**c** and **d**) Immunoblotting detection of BRK (c) and HIF1α (d) phosphorylation in MDA-MB-231 cells transfected with indicated LNA and expression vectors followed by HB-EGF stimulation. (**e**) qRT-PCR analysis of HIF1α target genes expression in MDA-MB-468 cells transfected with control or *LINK-A* siRNA followed by HB-EGF treatment. **(f)** qRT-PCR analyses of *LINK-A* expression level in MDA-MB-231 cells transfected with control shRNA or *LINK-A* shRNAs. **(g-i)** Lactate production (g and h) or glucose uptake (i) assay in MDA-MB-231 and MDA-MB-468 cells transfected with control or *LINK-A* siRNAs. **(j)** Cell proliferation rate was assessed by OD density (590 nm) in MDA-MB-231 cells transfected with LNAs as indicated. (**k** and **l)** Glucose uptake (k) or lactate production (l) was measured in MDA-MB-231 cells transfected with scramble or *LINK-A* LNAs. For panels **a-b**, **e-l**, error bars, S.E.M., n=3 independent experiments (n.s., p>0.05, *p<0.05, and **p<0.01, two-tailed paired Student's t-test). **(m)** Measurement of tumor volume in mice that were subcutaneously injected with MDA-MB-231 cells harboring control or *LINK-A* shRNA at indicated post-injection time point. Data are mean±S.E.M. n=5 mice *per* group (**p<0.01, two-tailed paired Student's t-test).

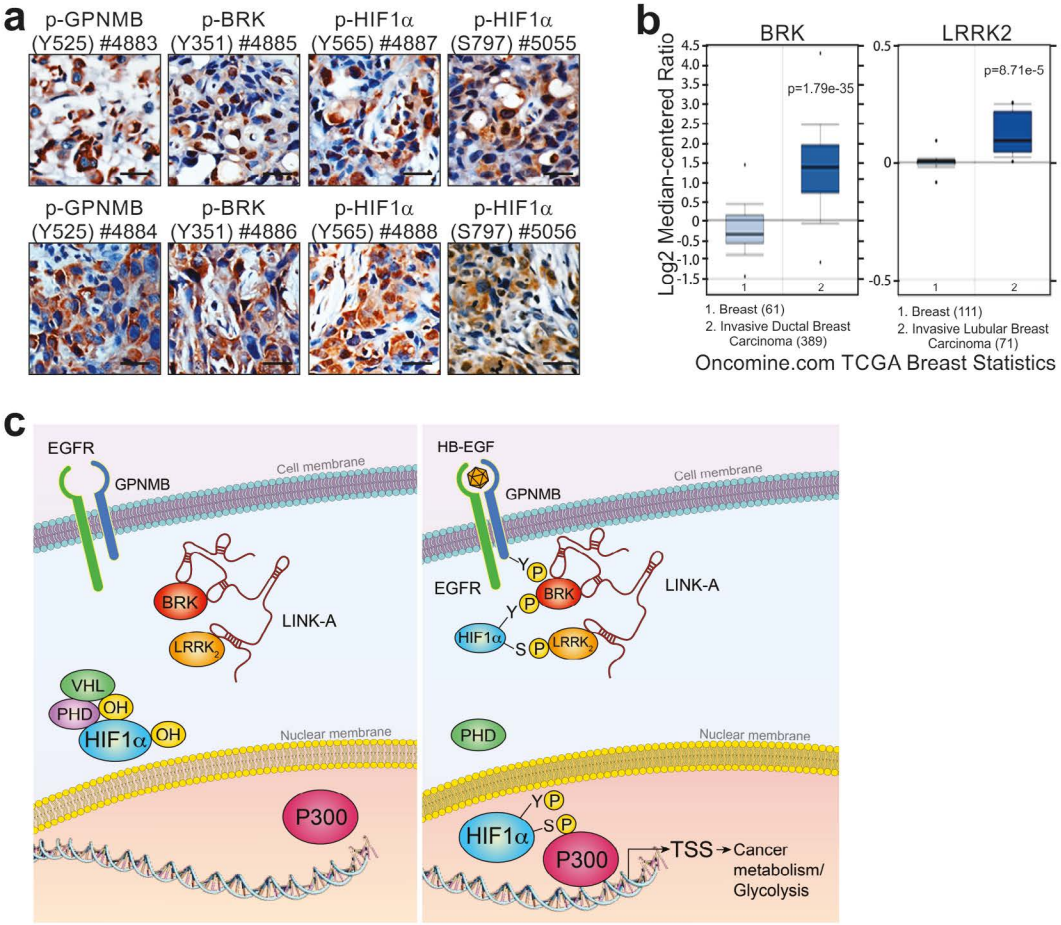

Supplementary Figure 6 Correlation of *LINK-A*-mediated signaling pathway activation with TNBC. **(a)** IHC staining of phospho-GPNMB (Tyr525), phospho-BRK (Tyr351), phospho-HIF1α (Tyr565) and phospho-HIF1α (Ser797) in human breast cancer tissues. Scale bars, 100μm. **(b)** Oncomine boxed plot showing BRK and LRRK2 expression levels in human normal and breast cancer tissues. **(c)** Graphic illustration of functional roles of *LINK-A* in HB-EGF-triggered, EGFR: GPNMB receptor-dependent and BRK/LRRK2-mediated HIF1α signaling cascade.

Fig.1h

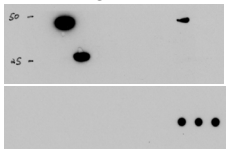

Fig.1i

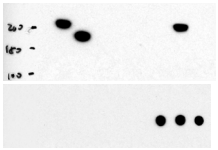

Fig.1j

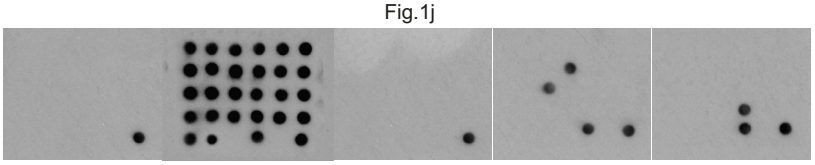

Fig.1k

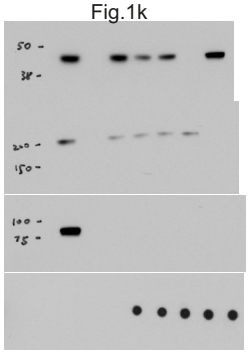

Fig.2b

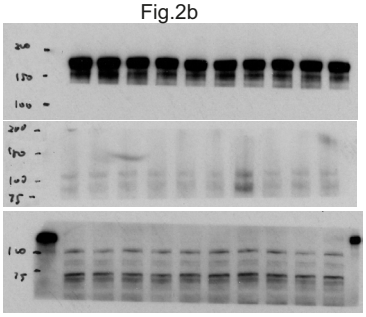

Fig.2c

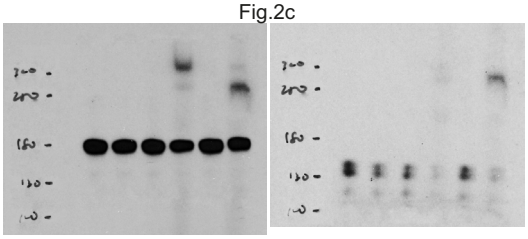

Fig.2f

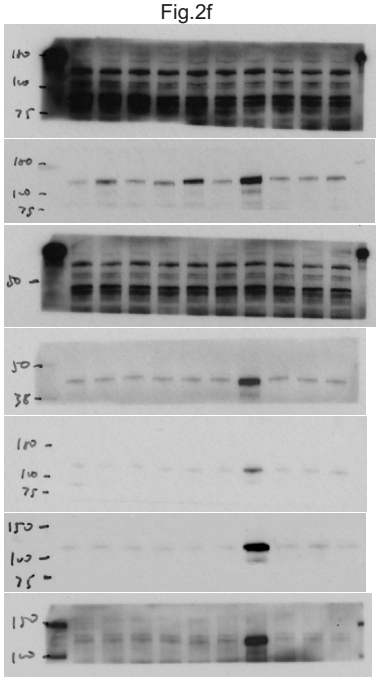

Fig.2d

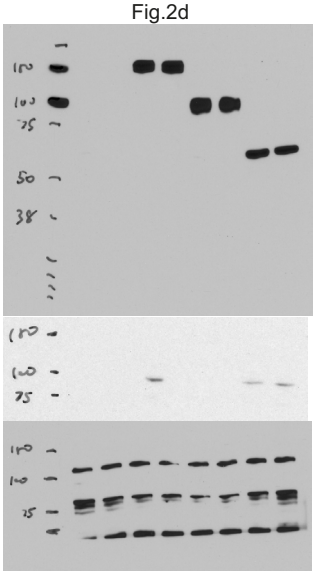

Fig.2e

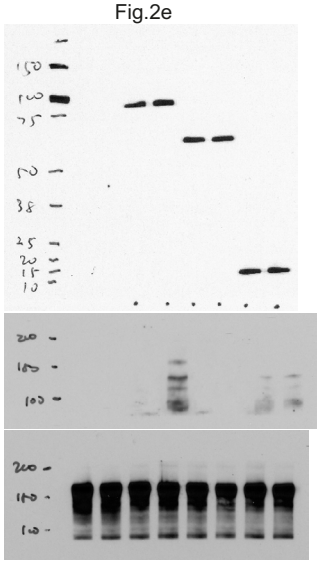

Fig.2g

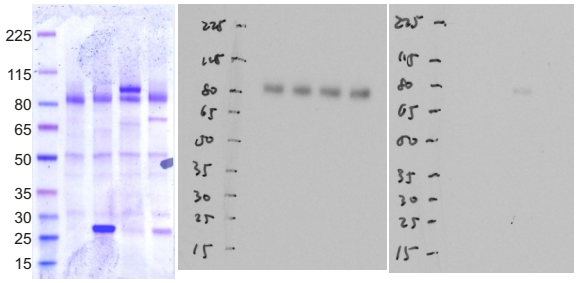

Fig.2h

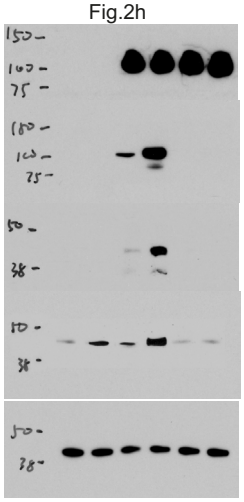

Fig.2i

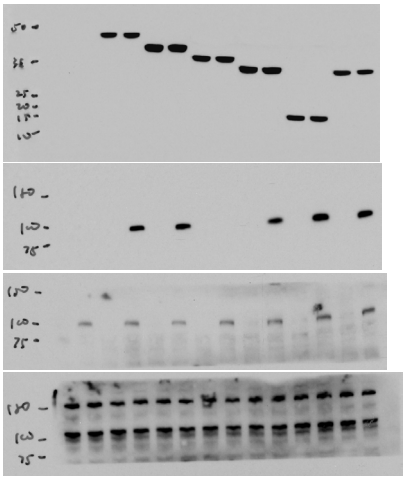

Supplementary Figure 7 Uncropped images for IB detection.

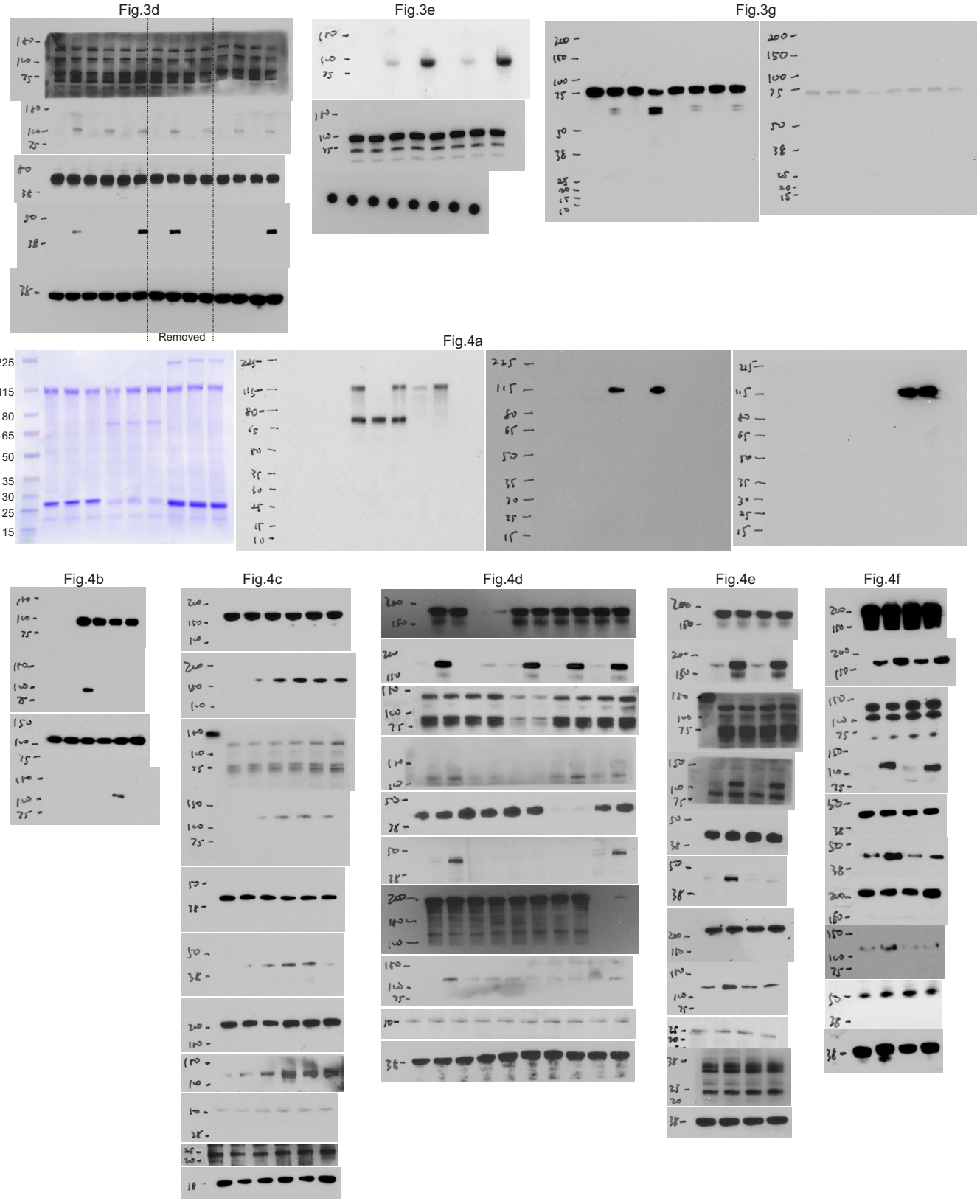

Supplementary Figure 7 continued

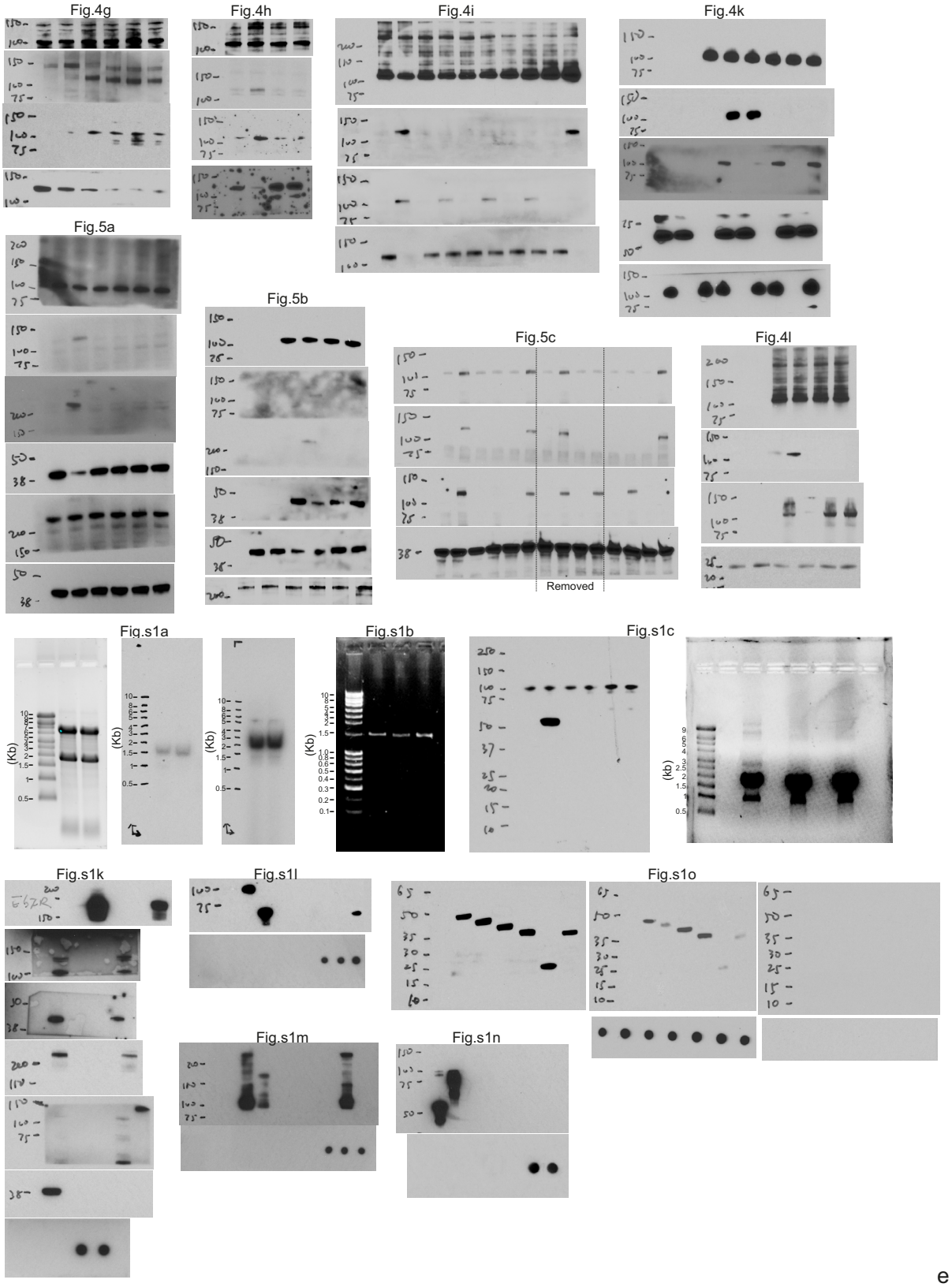

Supplementary Figure 7 continued

Fig.s2e

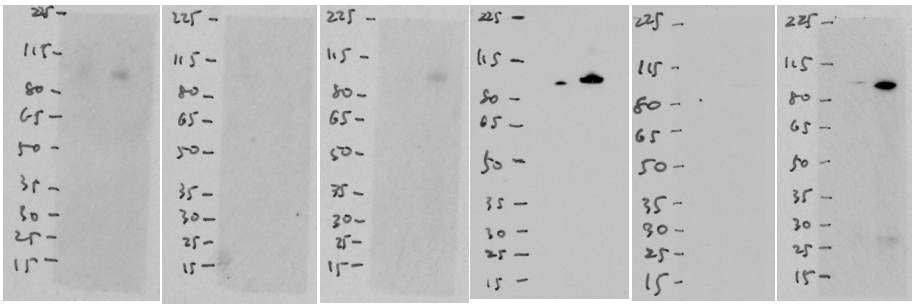

Fig.s2i

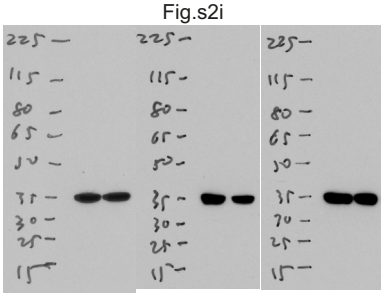

Fig.s2f

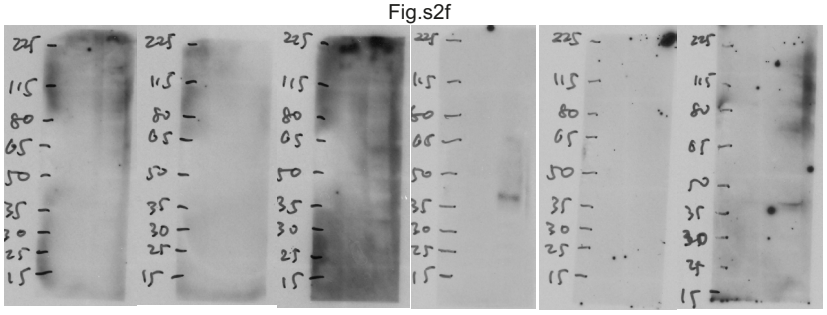

Fig.s2j

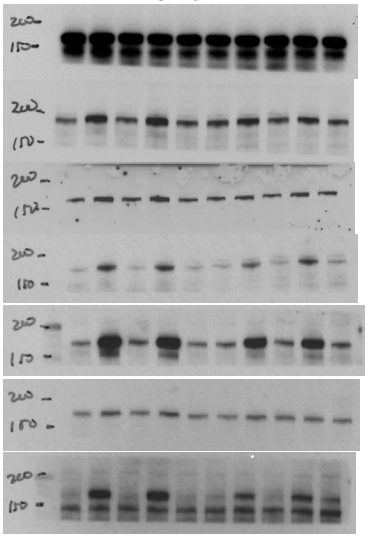

Fig.s2g

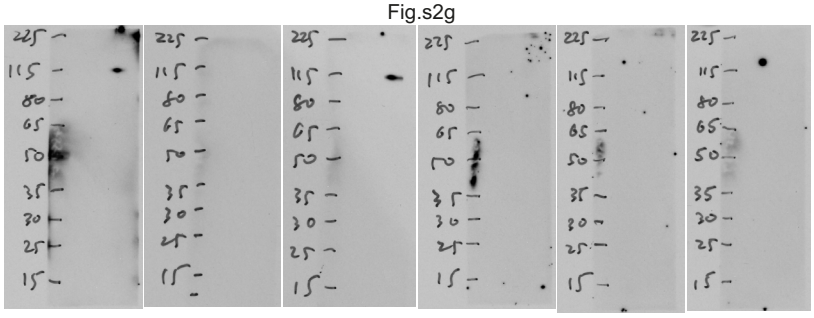

Fig.s2k

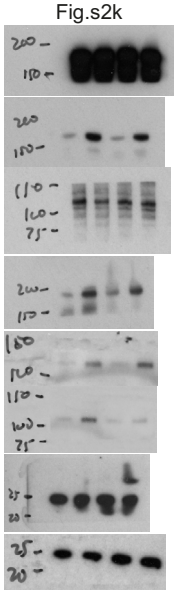

Fig.s2h

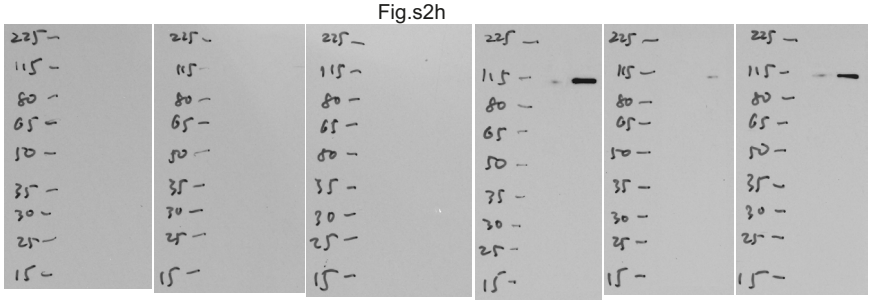

Fig.s2m

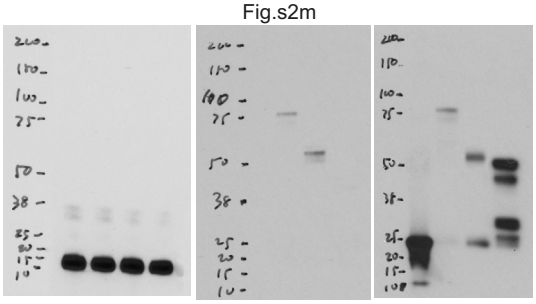

Fig.s4c

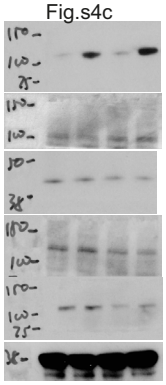

Fig.s4d

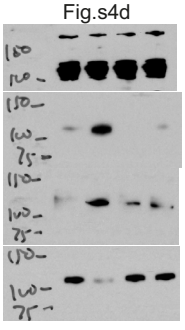

Supplementary Figure 7 continued

Fig.s2n

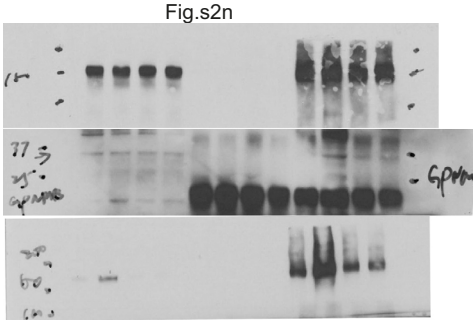

Fig.s2o

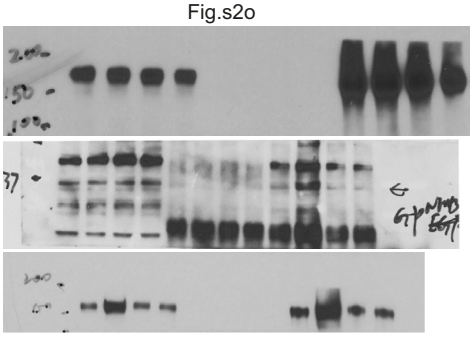

Fig.s4k

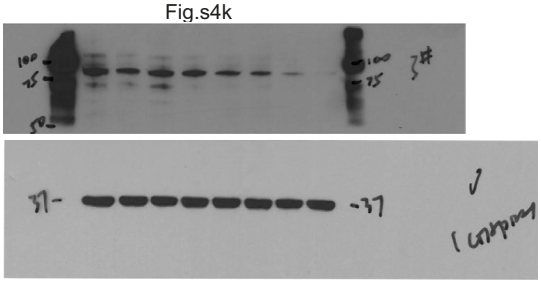

Fig.s4l

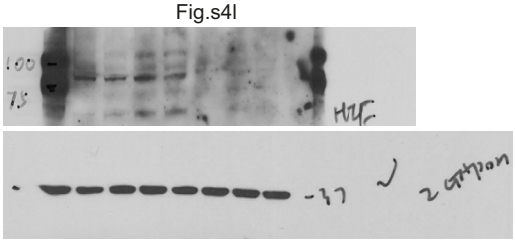

Fig.s4m

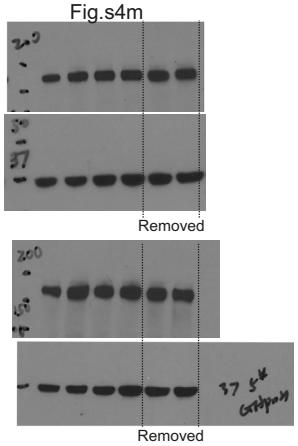

Fig.s4n

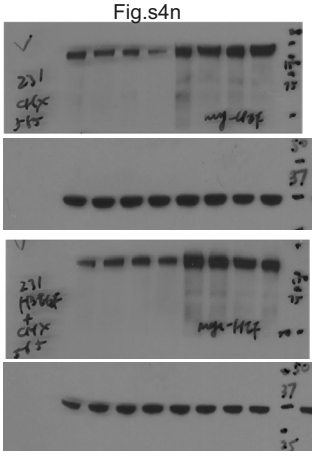

Fig.s4o

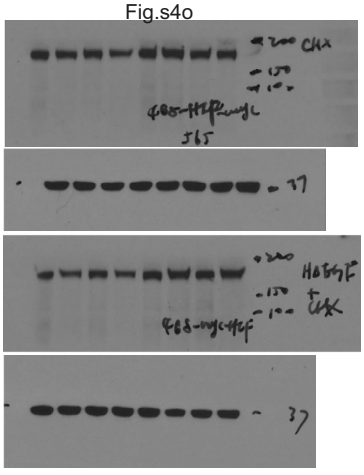

Fig.s5c

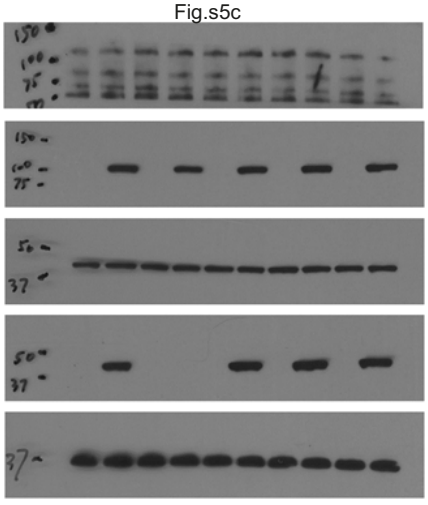

Fig.s5d

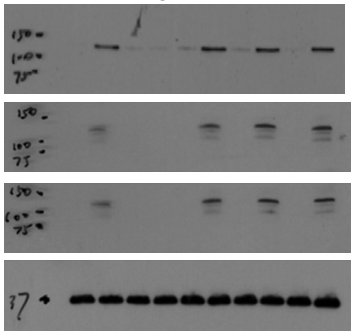

Supplementary Figure 7 continued

Supplementary Table Legends

Supplementary Table 1 Clinicopathological parameters of fresh frozen tissues and tissue microarrays used in this study.
BR487: Triple-negative breast cancer tissue array, including TNM, clinical stage and pathology grade, majority cases with negative of ER, PR, HER-2 in IHC, 48 cases/ 48 cores (Biomax);
Bre170Sur-01: Breast carcinoma, including TNM, clinical stage, pathology grade and survival information, 170 cases (160 cases have only tumor, 1 core/ case. 10 cases have only NAT, 1 core/case) (USbiolab);
T6235086-Frozen Tissue Array: 37 different breast tumors and 3 corresponding normal control (Biochain);
Duke University, Jeff Marks: 151 Frozen breast tumors samples with recurrence information, obtained123RNA isolation samples in all for qPCR assay and further recurrence free survival assay);
TMA007: Triple negative breast cancer tissue array, including TNM, clinical stage and pathology grade, majority cases with negative of ER, PR, HER-2 in IHC (Indivumed);
Nanjing Medical University: Breast cancer tissue array containing 20 breast cancer tissues (3 are triple negative), including TNM and clinical stage information, 20 cases/20 cores;
BRF404b: Frozen breast cancer tissue array with adjacent breast tissue as control, containing 17 cases of invasive ductal carcinoma and 3 cases of adjacent breast tissue, including TNM, clinical stage and pathology grade, 20 cases/40 cores (Biomax).

Supplementary Table 2 Protein identification results for biotinylated *LINK-A* pulldown experiments.
Complete mass spectrometry results for biotinylated ***LINK-A*** associated proteins pulled down from MDA-MB-231 cells. This file has three tabs, listing the number of unique and shared peptides identified for monoavidin magnetic beads, sense and antisense ***LINK-A*** RNA samples.

Supplementary Table 3 LC-MS analysis of *in vitro* hydroxylation assay with unphosphorylated or Tyr565- phosphorylated HIF1α peptide.
Complete mass spectrometry analysis results for ***in vitro*** hydroxylation assay with synthesized HIF1α peptide (557-566) (unphosphorylated ***vs***. Tyr565-phosphorylated) and PHD1 in the absence or presence of DMOG were shown.

Supplementary Table 4 Identification of genome-wide HIF1α occupancy in response to HB-EGF treatment.
Complete list of ChIP-seq peak calling of HIF1α upon HB-EGF stimulation in MDA-MB-231 cells using MACS version 1.4, with ***p*** value cut off (1.00e-04).